Applied Mathematical Modelling 37 (2013) 7245–7272

Contents lists available at SciVerse ScienceDirect

Applied Mathematical Modelling

journal homepage: www.elsevier.com/locate/apm

On optimization of the RBF shape parameter in a grid-free local scheme for convection dominated problems over non-uniform centers

Y.V.S.S. Sanyasiraju *, Chirala Satyanarayana

Department of Mathematics, Indian Institute of Technology Madras, Chennai 600 036, India

ARTICLE INFO

Article history:
Received 27 April 2012
Received in revised form 26 December 2012
Accepted 9 January 2013
Available online 5 March 2013

Keywords:
Grid-free scheme
Radial basis function
Convection–diffusion
Multi-quadric
Optimal shape parameter

ABSTRACT

Global optimization techniques exist in the literature for finding the optimal shape parameter of the infinitely smooth radial basis functions (RBF) if they are used to solve partial differential equations. However these global collocation methods, applied directly, suffer from severe ill-conditioning when the number of centers is large. To circumvent this, we have used a *local* optimization algorithm, in the optimization of the RBF shape parameter which is then used to develop a grid-free local (LRBF) scheme for solving convection–diffusion equations. The developed algorithm is based on the re-construction of the forcing term of the governing partial differential equation over the centers in a local support domain. The variable (optimal) shape parameter in this process is obtained by minimizing the *local* Cost function at each center (node) of the computational domain. It has been observed that for convection dominated problems, the local optimization scheme over uniform centers has produced oscillatory solutions, therefore, in this work the local optimization algorithm has been experimented over Chebyshev and non-uniform distribution of the centers. The numerical experiments presented in this work have shown that the LRBF scheme with the *local* optimization produced accurate and stable solutions over the non-uniform points even for convection dominant convection–diffusion equations.

1. Introduction

The radial basis function (RBF) based grid-free local schemes are becoming very attractive choice for solving fluid flow and heat transfer problems due to their better conditioning and flexibility in handling the non-linearities. Application of RBF based schemes to various equations governing diverse physical phenomena can be seen in [1–8]. When infinitely smooth RBFs are used in the computations then the shape parameter of these RBFs plays a very significant role in obtaining accurate and stable solutions. In most of the existing literature, researchers have chosen a constant optimal shape parameter over the full domain either by trail and error or by some ad hoc means and mostly validated over Poisson type equations. This strategy may not be good for the convection dominated convection diffusion equations (CDE), wherein clustering of the centers in the selected areas is necessary to capture the layer solutions accurately. Due to the high gradients of the solution in these regions, a variable shape parameter may be more suitable to produce accurate solutions.

The collocation matrices of the globally supported RBFs are highly dense and ill-conditioned when they are applied directly. The effect of ill-conditioning also increases with the number of centers. Recently Shu et al. [9], Wright and Fornberg [10], Chandini and Sanyasiraju [11] and Sanyasiraju and Chandini [12] used some RBF-based *local* schemes, by sacrificing the

* Corresponding author. Tel.: +91 44 22574621; fax: +91 44 22574602.
E-mail addresses: sryedida@iitm.ac.in (Y.V.S.S. Sanyasiraju), chiralasatya@gmail.com (C. Satyanarayana).

0307-904X/$ - see front matter © 2013 Elsevier Inc. All rights reserved.
http://dx.doi.org/10.1016/j.apm.2013.01.054

spectral accuracy which is inherent in the global collocation schemes. It has been observed that the local schemes produced better conditioned linear systems and also more flexible in handling the non-linearities.

According to Franke [13], MQ–RBF, $\phi(r) = \sqrt{(1+(\varepsilon r)^2}$, where $r = \|\underline{x}\|_2, \underline{x} \in \mathbb{R}^d, d-$ is the dimension of the problem, ε is the shape parameter, provides the best approximation, when compared with the other radial functions like Gaussian and Splines. However, recently Boyd [14] has compared Gaussian (GA), hyperbolic secant (HS), inverse quadrics (IQ), multiquadric (MQ) and inverse multiquadric (IMQ) and shown that the corresponding cardinal functions of these RBFs over uniform unbounded grid are all approximated by the same function.

For infinitely smooth RBF's like MQ, there is a *trade-off* [15] between the accuracy and conditioning due to the ill-conditioning of the direct computation at small values of ε. To produce stable solutions at small values of the shape parameter (flat RBFs), Fornberg and Wright [16] proposed Contour-Padè method and Fornberg and Piret [17] proposed RBF–QR method in which the former method is limited to work over small number of RBF centers and the latter one is developed to work for the centers distributed over the surface of a sphere. Recently Fornberg et al. [18], have presented stable computations with Gaussian RBF using RBF–QR method for one, two and three dimensional problems. Davydov and Oanh [19] developed an adaptive scheme based on RBF–QR method for Poisson equation. In these stable schemes, the flat RBF bases in the computations have been replaced with a well behaved bases that spans the same approximated space.

Another direction, to improve the accuracy of the computations, attempted by the researchers in the literature is the optimization of the shape parameter. For the interpolation with scattered data, there is some work on the optimal choice of the shape parameter based on the number of centers and the distance between them [13,20,21]. Rippa [22] proposed a "*leave-one-out cross-validation*" (LOOCV) algorithm, according to which the shape parameter should depend on the number of centers, distribution of centers, RBF interpolant (ϕ), condition number of the matrix and finally the machine precision. Kansa and Carlson [23], Fornberg and Zuev [24] proposed to use spatially variable shape parameters to improve the accuracy in MQ–RBF interpolation instead of the constant shape parameter. Fasshauer and Zhang [25] extended the LOOCV algorithm in finding the optimal shape parameter in pseudo-spectral (PS) methods. Roque and Ferreira [26] experimented the LOOCV algorithm to find the optimal shape parameter in global RBF collocation for solving partial differential equations. The global optimization techniques may be good for the problems having smooth solutions, however, they suffer from the ill-conditioning as the number of centers increase. For the problems like convection diffusion equations (CDE), particularly for convection dominated problems, special attention may be required in the choice of the numerical scheme, selection of the centers, and the optimization of the shape parameter, in order to get stable and accurate solutions.

The authors have proposed a *local* optimization algorithm to optimize the shape parameter of the Multi-quadric RBF used in the development of a grid-free *local* (LRBF) scheme [27]. The algorithm is based on the re-construction of the forcing term of the governing CDE using the collocation over the centers in a local support domain. In order to reduce the computational complexity of the proposed algorithm, Rippa's [22] LOOCV formula, which has been originally been developed for interpolation, has been extended to calculate the residual errors. The variable optimal shape parameter is obtained by minimizing the *local* Cost function at each center (node) of the computational domain. The *local* algorithm truly depends on the problem and the local distribution of the centers. The procedure is easy to implement and also can be used to find a constant shape parameter. The constant optimal shape parameter is obtained by minimizing the *global* Cost function, which is defined based on the average residual error over the full domain. In the present work, the *local* optimization algorithm is first validated using Poisson equations and then tested for one and two dimensional linear CDEs with strong boundary layer solutions over the Chebyshev and a non-uniform points and the results have been compared with the corresponding solutions obtained with uniform centers.

Rest of the paper is organized as follows. In Section 2, the derivation of the RBF grid-free *local* (LRBF) scheme is presented. In Section 3, the derivation of the *local* optimization algorithm to optimize the shape parameter is highlighted. In Sections 4 and 5, the numerical validation and verification of the developed algorithm is undertaken and finally, some concluding remarks are made in the last section.

2. Development of a grid-free *local* scheme using RBF's

In the local RBF scheme, the support for any reference node, $\underline{x}_i$, is pre-fixed as shown in Fig. 1 for any two-dimensional domain $d = 2$. Let $\mathscr{L}$ be a linear convection–diffusion operator defined in a domain, say, Ω, N be the total number of centers in the computational domain, then $\mathscr{L}u_i$, at any center '$\underline{x}_i$', is expressed as a linear combination of the function values u at $n_i(\ll N)$ centers $\mathbf{C}_i = \{\underline{x}_1, \underline{x}_2, \ldots, \underline{x}_{n_i}\}$ in the neighborhood of $\underline{x}_i$. Symbolically, this is given by

$$\mathscr{L}u(\underline{x}_i) \approx \sum_{j=1}^{n_i} c_j u(\underline{x}_j), \quad \text{for each} \quad \underline{x}_i \in \Omega \tag{1}$$

Then, the computation of the weights c_j gives the required approximation. To compute the weights c_j, consider the Lagrange's representation of RBF interpolant, for n_i nodes, given by

$$u(\underline{x}) \approx s(\underline{x}) = \sum_{j=1}^{n_i} \psi_j(\underline{x}) u(\underline{x}_j) \tag{2}$$

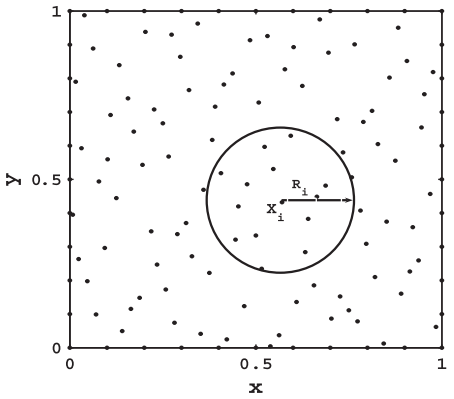

Fig. 1. Schematic diagram of the local RBF stencil.

where $\psi_j(\underline{x})$'s satisfy the cardinal conditions

$$\psi_j(\underline{x}_k) = \delta_{jk}, \quad j,k = 1,2,\ldots,n_i \tag{3}$$

The closed form representation for $\psi_j(\underline{x})$, in terms of $\phi(\|\underline{x}-\underline{x}_j\|,\varepsilon)$'s, and the polynomial basis, $\{p_j(\underline{x})\}_{j=1}^{l}$, $l = \binom{d+m-1}{m-1}$, where m is the order of ϕ (for MQ, $m=1$), is found by constructing a set of RBF interpolation problems for which the data is obtained from the cardinal conditions on ψ_j. That is,

$$\psi_j(\underline{x}) = \frac{det(A_j(\underline{x}))}{det(A)}, \text{ where } A(\underline{x}) = \begin{bmatrix} \Phi & \mathbf{p} \\ \mathbf{p}^T & \mathbf{0} \end{bmatrix} \tag{4}$$

where $\Phi := \phi(\|\underline{x}_i - \underline{x}_j\|,\varepsilon)$, $i,j = 1,2,\ldots,n_i$, $\mathbf{p}_{i,j} := p_j(\underline{x}_i)$, $j = 1,2,\ldots,l, i = 1,2,\ldots,n_i$, $A_j(\underline{x})$ is same as the matrix A with size $(n_i + l)$, except that jth row is replaced by the vector

$$B(\underline{x}) = [\phi(\|\underline{x}-\underline{x}_1\|,\varepsilon),\ldots,\phi(\|\underline{x}-\underline{x}_{n_i}\|,\varepsilon)|p_1(\underline{x}),\ldots,p_l(\underline{x})] \tag{5}$$

The representation derived through (2)–(4) can be used to approximate the derivatives of a function or in general, values of $\mathscr{L}u$ at a given set of centers, say $\underline{x}_i$. Applying the operator $\mathscr{L}$ to the Lagrange's representation of RBF interpolant (2) gives

$$\mathscr{L}u(\underline{x}_i) \approx \mathscr{L}s(\underline{x}_i) = \sum_{j=1}^{n_i} \mathscr{L}\psi_j(\underline{x}_i)u(\underline{x}_j) \tag{6}$$

Comparing Eqs. (1) and (6), gives

$$c_j = \mathscr{L}\psi_j(\underline{x}_i) = \mathscr{L}\frac{det(A_j(\underline{x}_i))}{det(A)}, \quad j = 1,2,\ldots,n_i \tag{7}$$

If c_j's are as given in (7), then using the Cramer's rule backwards they can also be obtained by solving the linear system (refer [12], for the complete derivation),

$$A[\mathbf{c}/\bar{\gamma}] = (\mathscr{L}B(\underline{x}_i))^T, \quad \text{for each} \quad \underline{x}_i \in \Omega \tag{8}$$

where A is a matrix given in (4), $B(\underline{x})$ is a vector given in (5) and $\mathbf{c}$ is the vector containing the weights. A similar procedure is applied to discretize the boundary operator $\mathscr{B}$. For any center $\underline{x}_i \in \Omega \cup \partial\Omega$, the system (8) is of size only $n_i + l$ and can be solved using any direct method say, Gauss elimination. It is clear from the development of the final linear system (8) that, though it is dense, the size $(n_i + l)$ is very small, that makes the system more stable for a wide range of ε. Further, only the right-hand side of (8) depends on the operator $\mathscr{L}$, for which the weights are to be computed. This optimizes the computation, if the weights have to be computed for many operators with the same distribution of the centers, as in the case of non-linear equations.

3. A local algorithm for optimization of the shape parameter

The procedure given in the earlier section for the descritization of any differential operator, at any center $\underline{x}_i$, highly depends on the nature of the basis function. Therefore, the LRBF scheme, developed in the earlier section, is made more accurate by incorporating the optimization of its shape parameter. The complete derivation of the *local* optimization algorithm, initially been proposed in [27] (also refer [22]), however over Chebyshev and a set of non-uniform points is as follows:

The collocation conditions, when the collocation is used at any center $\underline{x}_i \in \Omega$ over a local support domain $\mathbf{C}_i$, are given by $\{\underline{x}_j, f(\underline{x}_j) = \mathscr{L}u(\underline{x}_j)\}_{j=1}^{n_i}$.

Let

$$\mathbf{C}_i^{(k)} = \{\underline{x}_1, \ldots, \underline{x}_{(k-1)}, \underline{x}_{(k+1)}, \ldots, \underline{x}_{n_i}\}$$

$$f_i^{(k)} = \{f_i(\underline{x}_1), \ldots, f_i(\underline{x}_{(k-1)}), f_i(\underline{x}_{(k+1)}), \ldots, f_i(\underline{x}_{n_i})\} \tag{9}$$

be the set of data points and their function values f, respectively, after removing the k-th center and its function value from the support $\mathbf{C}_i$. Then the forcing term f can be re-constructed, locally over $\mathbf{C}_i^{(k)}$ using the collocation, as

$$\widehat{f}_i^{(k)}(\underline{x}) = \sum_{j=1(j\neq k)}^{n_i+l} \mu_{i,j}^{(k)} (\mathscr{L}\phi)_j(\underline{x}) \tag{10}$$

where j is the local index, i is the global index, and the basis vector, $(\mathscr{L}\phi)(\underline{x})$ is given by,

$$(\mathscr{L}\phi)(\underline{x}) = [\mathscr{L}^2\phi(\|\underline{x} - \underline{x}_1\|, \varepsilon), \ldots, \mathscr{L}^2\phi(\|\underline{x} - \underline{x}_{n_i}\|, \varepsilon), p_1(\underline{x}), \ldots, p_l(\underline{x})] \tag{11}$$

$\mathscr{L}^2$ is a linear differential operator applied on RBF as a function of the second argument (center). It is a common practice in the RBF literature to add the polynomial basis $\{p_j(\underline{x})\}_{j=1}^{l}$ in (11) which requires additional l conditions

$$\sum_{j=1(j\neq k)}^{n_i} \mu_{i,j}^{(k)} p_{i'}(\underline{x}_j) = 0, \quad i' = 1, 2, \ldots, l \tag{12}$$

The coefficients, $\mu_i^{(k)} = (\mu_{i,1}^{(k)}, \ldots, \mu_{i,(k-1)}^{(k)}, \mu_{i,(k+1)}^{(k)}, \ldots, \mu_{i,n_i+l}^{(k)})^T$, in the Eq. (10) can be obtained by imposing the collocation conditions

$$\widehat{f}_i^{(k)}(\underline{x}_j) = f_i^{(k)}(\underline{x}_j), \quad j = 1, 2, \ldots, n_i, j \neq k \tag{13}$$

and the orthogonality conditions (12). Mathematically it is equivalent to solving the nonsingular linear system

$$A_{\mathscr{L}}^{(k)} \mu_i^{(k)} = F_i^{(k)} \tag{14}$$

where $A_{\mathscr{L}}^{(k)}$ is obtained, after removing the k-th row and the k-th column, from the collocation matrix,

$$A_{\mathscr{L}} = \begin{bmatrix} \mathscr{L}^2\Phi & \mathbf{p} \\ \mathbf{p}^T & \mathbf{0} \end{bmatrix} \text{ and } F_i = (f_i, \mathbf{0})^T \tag{15}$$

System (15) uses the data, over $\mathbf{C}_i, F_i^{(k)} = (f_i^{(k)}, \mathbf{0})^T$, $\mathscr{L}^2\Phi := \mathscr{L}^2\phi(\|\underline{x}_{i'} - \underline{x}_j\|, \varepsilon), i', j = 1, 2, \ldots, n_i$ and $\mathbf{p}_{i'j} := p_j(\underline{x}_{i'})$, $j = 1, 2, \ldots, l, i' = 1, 2, \ldots, n_i$.

If $f_i(\underline{x}_k)$ is the function value at the point that has been removed from $\mathbf{C}_i$ and $\widehat{f}_i^{(k)}(\underline{x}_k)$ is the corresponding reconstructed value using (10) then the residual error, $r_{i,k}$, can be computed using

$$r_{i,k}(\varepsilon) = f_i(\underline{x}_k) - \widehat{f}_i^{(k)}(\underline{x}_k), \quad k = 1, 2, \ldots, n_i \tag{16}$$

For each center $\underline{x}_i \in \Omega$, (16) gives residual errors for $k = 1, 2, \ldots, n_i$, therefore it requires $O((n_i + l)^4)$ operations for each center. To reduce the computational complexity, the Rippa's [22] formula, has been suitably modified to calculate the residual errors of the local optimization algorithm. This formula is originally been developed for the interpolation and also with out any polynomial augmentation. In the present work, the polynomial augmentation is included to guarantee the non-singularity of the obtained collocation matrix. The modification of the Rippa's interpolation formula [22] to the local collocation is as follows:

If $y_i = (y_{i,1}, y_{i,2}, \ldots, y_{i,n_i+l})^T$ and $z_i = (z_{i,1}, z_{i,2}, \ldots, z_{i,n_i+l})^T$ are such that $y_{i,k} = 0$, then we have

$$A_{\mathscr{L}}\, y_i = z_i \Rightarrow A_{\mathscr{L}}^{(k)}\, y_i^{(k)} = z_i^{(k)} \tag{17}$$

Then, consider the solution $x_i^{[k]}$ to the system

$$A_{\mathscr{L}}\, x_i^{[k]} = e_i^{[k]} \tag{18}$$

where $e_i^{[k]}$ is the k-th column of the $(n_i + l) \times (n_i + l)$ identity matrix. It is easy to verify that $x_{i,k}^{[k]} \neq 0$. Indeed, if $x_{i,k}^{[k]} = 0$, then by (17) and (18), we have

$$A_{\mathscr{L}}^{(k)}(x_{i,1}^{[k]}, \ldots, x_{i,(k-1)}^{[k]}, x_{i,(k+1)}^{[k]}, \ldots, x_{i,n_i+l}^{[k]})^T = \mathbf{0} \tag{19}$$

which implies, from the non-singularity of $A_{\mathscr{L}}^{(k)}$, that, $x_i^{[k]} = 0$. This is impossible because $x_i^{[k]}$ is the solution of (18). Consider the vector $b_i^{[k]} = (b_{i,1}^{[k]}, b_{i,2}^{[k]}, \ldots, b_{i,n_i+l}^{[k]})^T$, defined by

$$b_i^{[k]} = \mu_i - \frac{\mu_{i,k}}{x_{i,k}^{[k]}} x_i^{[k]} \tag{20}$$

Then we have

$$A_{\mathscr{L}} b_i^{[k]} = A_{\mathscr{L}} \mu_i - \frac{\mu_{k,i}}{x_{i,k}^{[k]}} A_{\mathscr{L}} x_i^{[k]} = F_i - \frac{\mu_{i,k}}{x_{i,k}^{[k]}} e_i^{[k]} \tag{21}$$

$$= \left(f_{i,1}, \ldots, f_{i,(k-1)}, f_{i,k} - \frac{\mu_{i,k}}{x_{i,k}^{[k]}}, f_{i,(k+1)}, \ldots, f_{i,n_i}, 0, \ldots, 0 \right)^T \tag{22}$$

And, since $b_{i,k}^{[k]} = 0$, we use (17) once again to conclude that

$$\mu_i^{(k)} = (b_{i,1}^{[k]}, \ldots, b_{i,(k-1)}^{[k]}, b_{i,(k+1)}^{[k]}, \ldots, b_{i,n_i+l}^{[k]})^T \tag{23}$$

This implies that,

$$\widehat{f}_i^{(k)}(\underline{x}_k) = \sum_{j=1(j\neq k)}^{n_i+l} \mu_{i,j}^{(k)} (\mathscr{L}\phi)_j(\underline{x}_k) = \sum_{j=1(j\neq k)}^{n_i+l} b_{i,j}^{[k]} (\mathscr{L}\phi)_j(\underline{x}_k) = \sum_{j=1}^{n_i+l} b_{i,j}^{[k]} (\mathscr{L}\phi)_j(\underline{x}_k) = (A_{\mathscr{L}} b_i^{[k]})_k = f_{i,k} - \frac{\mu_{i,k}}{x_{i,k}^{[k]}} \tag{24}$$

Using (24) in the Eq. (16), the residual error, $r_{i,k}$, also can be obtained by

$$r_{i,k}(\varepsilon) = \frac{\mu_{i,k}}{(A_{\mathscr{L}}^{-1})_{kk}}, \quad k = 1, 2, \ldots, n_i, \quad \text{for each} \quad \underline{x}_i \in \Omega \tag{25}$$

where $\mu_{i,k}$ is the k-th component in the vector μ_i and $(A_{\mathscr{L}})_{kk}^{-1}$ is the kth diagonal element of the inverse of the collocation matrix $A_{\mathscr{L}}$. Since (25) requires the inversion only once, the computational complexity is now $O((n_i + l)^3)$. By adopting a similar procedure for the boundary operator, $\mathscr{B}$, the residual error is computed using

$$r_{i,k}(\varepsilon) = \frac{\mu_{i,k}}{(A_{\mathscr{B}}^{-1})_{kk}}, \quad k = 1, 2, \ldots, n_i, \quad \text{for each} \quad \underline{x}_i \in \partial\Omega \tag{26}$$

Eqs. (25) and (26) can be used to calculate the optimal shape parameter in the following way:

3.1. Optimization of the shape parameter

Using Eqs. (25) and (26), define the (*global*) cost function as

$$\text{global}cost(\varepsilon) = \left(\frac{1}{N} \sum_{i=1}^{N} \|R_i\|_2^2 \right)^{1/2} \tag{27}$$

where the vector $R_i = (r_{i,k}(\varepsilon)/n_i), k = 1, 2, \ldots, n_i$ for each i and N is the total number of centers in the domain. By minimizing the (global) cost function (27), which is realized using the `fminbnd` function in MATLAB, the (near) optimal shape parameter is obtained.

The global cost functions those exist in the literature are prone to severe ill-conditioning due to their size, however, the (global) cost function (27) is better conditioned than such functions. In the present case, the size of the coefficient matrices, $A_{\mathscr{L}}, A_{\mathscr{B}}$, in the Eqs. (25), (26) is only $(n_i + l)$ which is vary small, when compared to the size $(N + l)$ of the existing global collocation matrices. The smaller size makes the present system more stable for wide range of shape parameters.

For different values of the shape parameter (ε), in the neighborhood of the optimal shape parameter, the (global) Cost function (27) has been compared with the (RMS) error function of various test problems to show that the pattern of global cost function with respect to different shape parameters is similar to that of the RMS error function. The RMS error function, for different test problems, is calculated using

$$\text{RMS error}(\varepsilon) = \left(\frac{1}{N} \sum_{i=1}^{N} |\text{Analytical solution}(i) - \text{LRBF solution}(i)|^2 \right)^{1/2} \tag{28}$$

Due to the similarity of their pattern, minimizing the global cost function leads to minimization of the RMS error function which can't be computed unless the exact solution of the test problem is known.

The optimized shape parameter obtained from the minimization of the (global) cost function is then compared with the best shape parameter which has been defined as the value of the shape parameter at which the error function is minimum. One should note that the best shape parameter can be obtained only when the analytical solution of the problem is known.

Therefore, the purpose of the computation of the global cost function is twofold. One is to compare with the error function to show the similarity of their patterns and the other is to compare its optimum value with the best shape parameter. The two comparisons of the cost function given above verbalize the best solution one can obtain with a constant shape parameter and the next task is to experiment with a variable shape parameter obtained as follows:

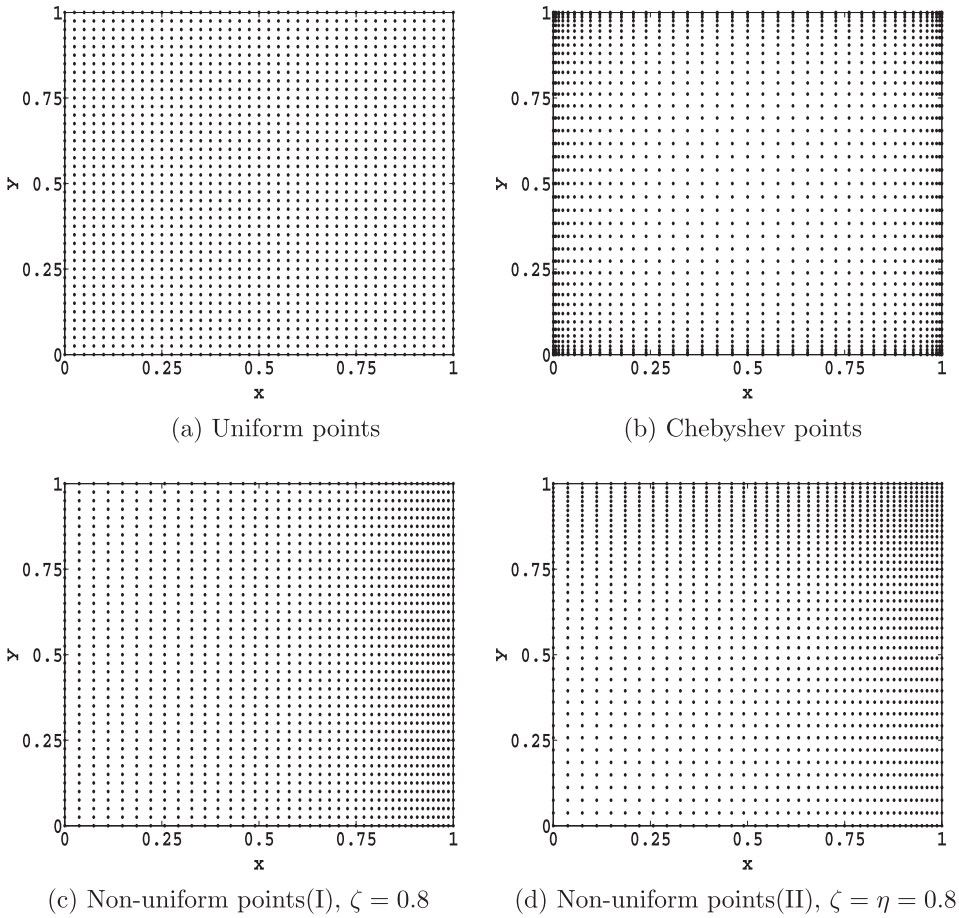

Fig. 2. Centers in two-dimensional computational domain ($N = 41 \times 41$).

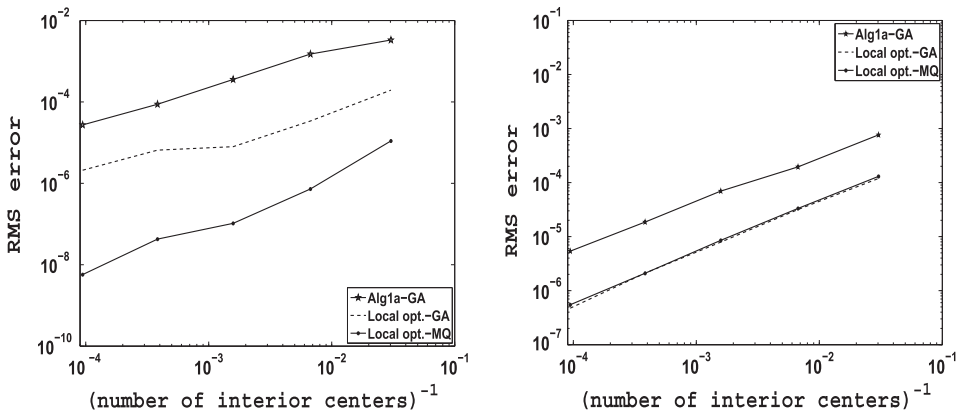

Fig. 3. Comparison of RMS errors with the present and [28] (Figs. 8(a) and 10(c) of [28]) with the Gaussian and Multiquadric RBFs. (a) Problem P1, (b) problem P2.

Define a (*local*) Cost function

$$\text{local}\,cost(\varepsilon_i) = \|R_i\|_2 \tag{29}$$

where the vector $R_i = (r_{i,k}(\varepsilon)/n_i), k = 1, 2, \ldots, n_i$ and $r_{i,k}(\varepsilon)$ is as given in Eqs. (25), (26) for every $\underline{x}_i \in \Omega$ or $\underline{x}_i \in \partial\Omega$, respectively. In this process, the (near) optimal shape parameter is calculated by minimizing the (local) Cost function at each center of the computational domain. Therefore, this procedure gives a variable shape parameter as a function of $\underline{x}$.

4. Numerical validation

The developed scheme is first validated over the following two Poisson equations taken from [28].

1. *Poisson problem* P_1

$$u_{xx} + u_{yy} = -2\pi^2 sin(\pi x) sin(\pi y), \quad 0 < x, \ y < 1 \tag{30}$$

$$u(x, y) = sin(\pi x) sin(\pi y) \tag{31}$$

2. *Poisson problem* P_2

$$u_{xx} + u_{yy} = (y^2 + (-2x + 0.2)^2 - 3) e^{-(x-0.1)^2 - 0.5y^2}, \quad 0 < x, \ y < 1 \tag{32}$$

$$u(x, y) = e^{-(x-0.1)^2 - 0.5y^2} \tag{33}$$

In [28], Poisson problems P1 and P2 have been solved using Gauss – QR algorithm with optimum shape parameter. Therefore, by validating the developed scheme over these problems with the best solutions presented in [28] demonstrates the accuracy of the developed scheme for the linear diffusion problems. Further, these comparisons have been carried out using both multiquadric and Gaussian RBFs, so that the better RBF, in terms of accuracy, can be used in the later computations with CDE. By varying the number of centers, the RMS errors obtained with the developed scheme, for the problems P1 and P2, have been compared in the Fig. 3. The *Alg*1*a_GA* curves presented in these figures are the best solutions (among the two algorithms presented) obtained in [28]. It is clear from these comparisons that for both the problems, the RMS errors obtained with the present scheme are much smaller than the literature values. Further, for problem P1, the MQ solution is better than the solution obtained with GA but for the second problem P2, both RBFs gave similar solutions.

5. Numerical experiments with CDE

After validating with the Poisson problems, the following one and two dimensional convection dominated CDEs, two for each case, with known analytical solutions are chosen to experiment the LRBF scheme with the developed optimization algorithms. The forcing term and the Dirichlet boundary conditions are taken from the analytical solutions where ever they are needed.

Table 1
Comparison of RMS errors obtained using Multiquadric (MQ) and Gaussian (GA) RBFs with local optimal shape parameters calculated over the uniform, Chebyshev and the non-uniform points for the Test problem 1, at $N = 81$.

	$N \rightarrow$	Uniform points		Chebyshev points		Non-uniform points	
		MQ	GA	MQ	GA	MQ	GA
$a = 10^{-2}$	Local	(5.4285, 11.4600)	(0.9935, 0.9936)	(0.12, 0.8118)	(0.9926, 0.9937)	(0.6624,1.1373)	(0.9934, 0.9937)
	RMS error	6.65(−3)	6.10(−3)	3.31(−3)	2.49(−3)	1.36(−3)	1.06(−3)
$a = 10^{-3}$	Local	(0.7860, 0.8107)	(0.9935, 0.9936)	(0.3662, 2.2537)	(0.9930, 0.9937)	(0.6483, 2.1634)	(0.9934, 0.9938)
	RMS error	1.17(−1)	1.17(−1)	2.85(−2)	1.03(−2)	3.85(−3)	4.04(−3)
$a = 10^{-4}$	Local	(0.8102, 1.010)	(0.9931, 0.9935)	(0.01, 0.8447)	(0.9934, 0.9937)	(0.8313, 1.8686)	(0.9934, 0.9938)
	RMS error	4.78(−1)	4.75(−1)	3.33(−2)	3.84(−2)	6.67(−3)	5.36(−3)

Table 2
Comparison of RMS errors obtained using Multiquadric (MQ) and Gaussian (GA) RBFs with local optimal shape parameters calculated over the uniform, Chebyshev and the non-uniform points for the Test problem 1, at $N = 161$.

	$N \rightarrow$	Uniform points		Chebyshev points		Non-uniform points	
		MQ	GA	MQ	GA	MQ	GA
$a = 10^{-2}$	Local	(1.1369, 2.5124)	(0.9934, 0.9936)	(0.4289, 2.9084)	(0.9932, 1.6421)	(0.7360, 1.2639)	(0.9934, 0.9935)
	RMS error	1.67(−3)	1.65(−3)	9.26(−4)	9.89(−4)	2.92(−4)	2.65(−4)
$a = 10^{-3}$	Local	(0.7860, 1.0831)	(0.9934, 0.9935)	(0.3673, 1.5000)	(0.9866, 1.3508)	(0.6964, 3.4399)	(0.9920, 0.9951)
	RMS error	4.76(−2)	4.75(−2)	3.80(−3)	5.92(−3)	4.91(−4)	3.01(−4)
$a = 10^{-4}$	Local	(0.8298, 1.0373)	(0.9930, 0.9934)	(0.2118, 0.8354)	(0.9908, 0.9985)	(0.5114, 2.1113)	(0.9930, 0.9969)
	RMS error	2.14(−1)	2.13(−1)	3.76(−3)	3.13(−3)	1.01(−3)	9.16(−4)

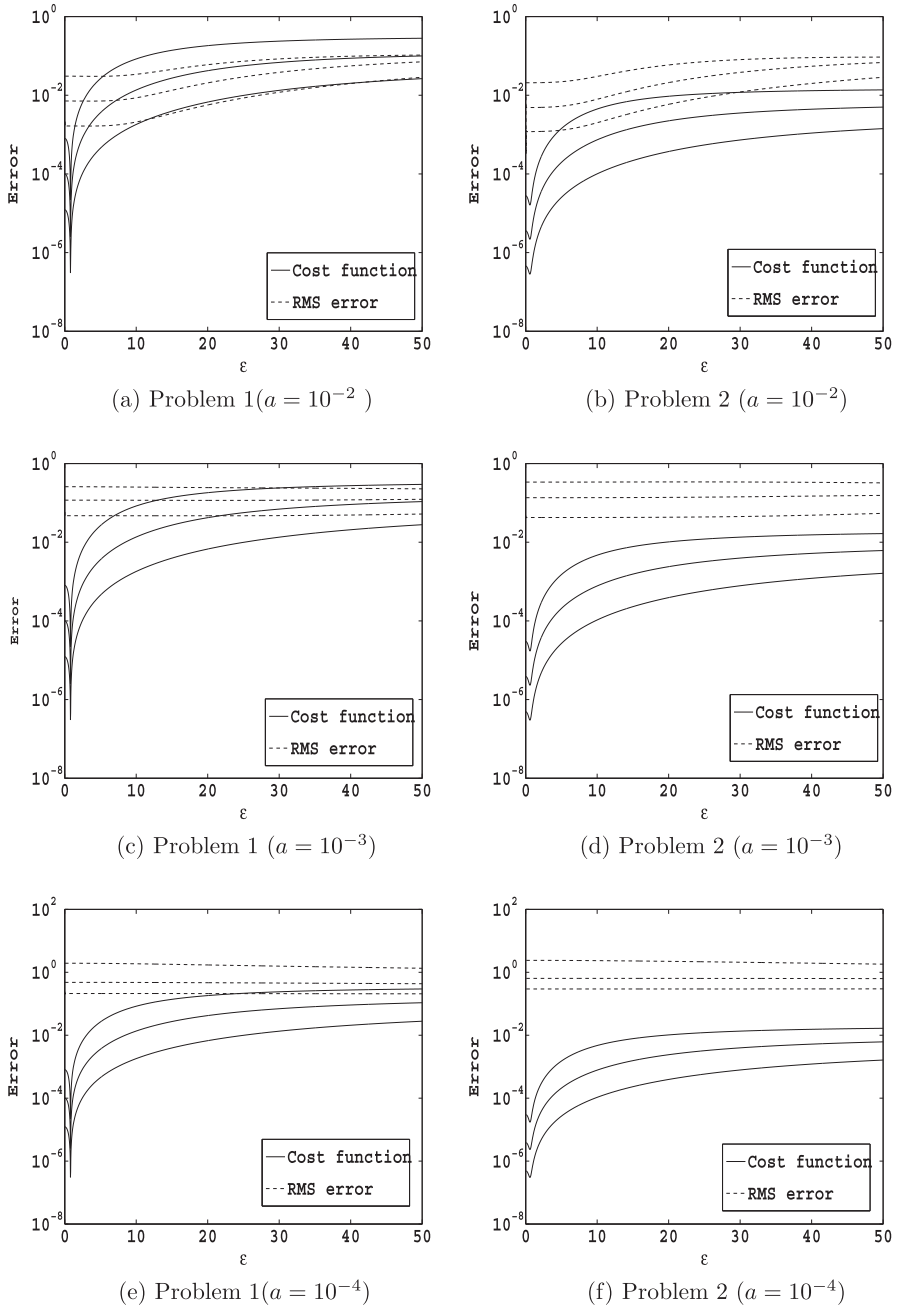

(a) Problem 1($a = 10^{-2}$) (b) Problem 2 ($a = 10^{-2}$)

(c) Problem 1 ($a = 10^{-3}$) (d) Problem 2 ($a = 10^{-3}$)

(e) Problem 1($a = 10^{-4}$) (f) Problem 2 ($a = 10^{-4}$)

Fig. 4. Comparison of RMS error & (*global*) Cost function against the Shape parameter for the Test problems 1 and 2, at $N = 41, 81, 161$ (from the top to bottom) over the uniform points.

Test problem 1

$$u_x - au_{xx} = \pi^2 asin(\pi x) + \pi cos(\pi x),\ \ 0 < x < 1,\ \ u(0) = 0, u(1) = 1 \quad \text{with} \tag{34}$$

$$u(x) = sin(\pi x) + \frac{e^{x/a} - 1}{e^{1/a} - 1} \tag{35}$$

Test problem 2

$$\frac{1}{1+x}u_x - au_{xx} = \left(\frac{1}{1+x} - a\right)e^x, \quad 0 < x < 1 \quad \text{with} \tag{36}$$

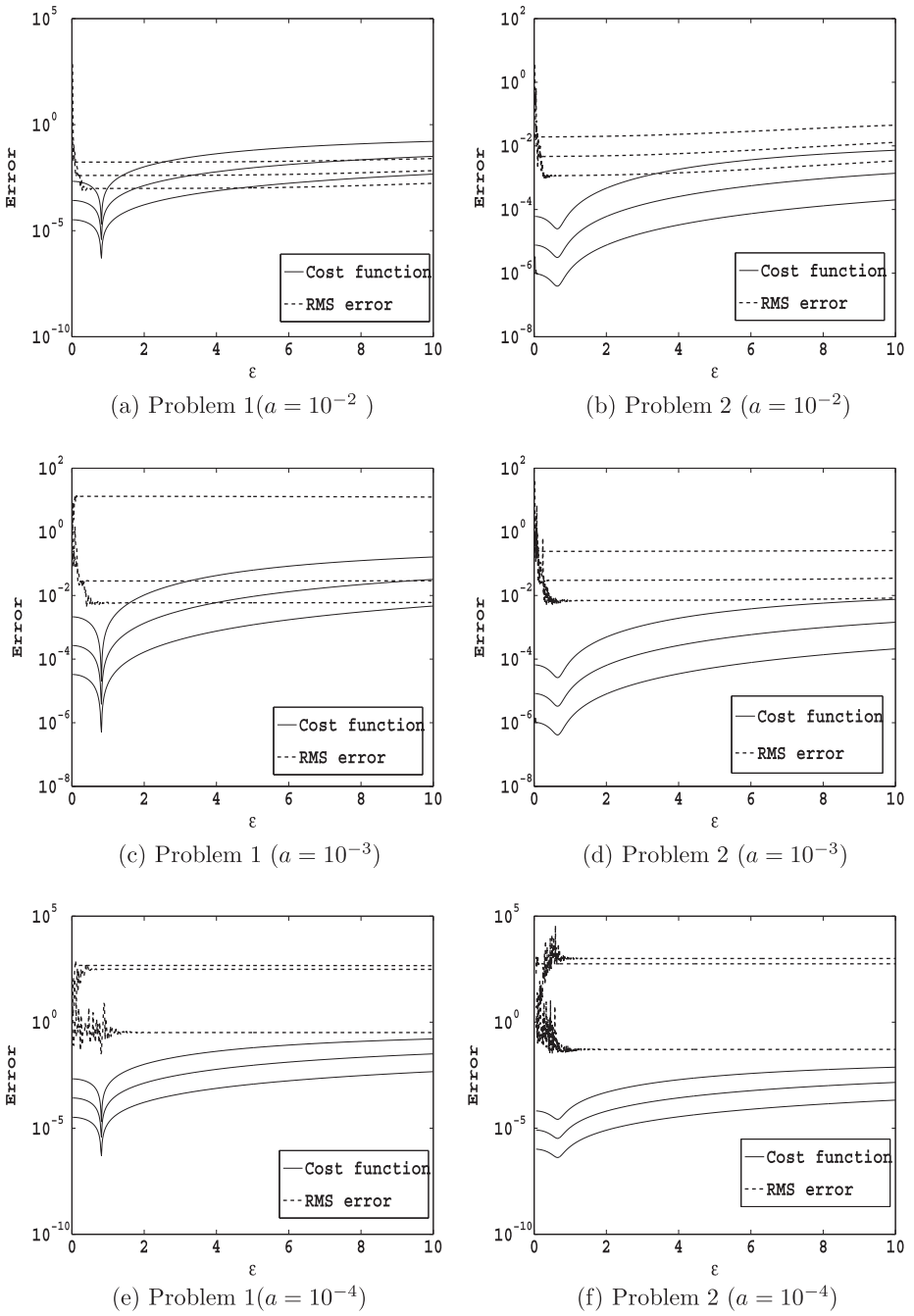

(a) Problem 1($a = 10^{-2}$) (b) Problem 2 ($a = 10^{-2}$)

(c) Problem 1 ($a = 10^{-3}$) (d) Problem 2 ($a = 10^{-3}$)

(e) Problem 1($a = 10^{-4}$) (f) Problem 2 ($a = 10^{-4}$)

Fig. 5. Comparison of RMS error & (*global*) Cost function against the Shape parameter for the Test problems 1 and 2, at $N = 41, 81, 161$ (from the top to bottom) over the Chebyshev points.

$$u(0) = 1 + 2^{-1/a}, u(1) = e + 2, \quad u(x) = e^x + 2^{-1/a}(1+x)^{(1+1/a)} \tag{37}$$

Test problem 3

$$2u_x - a(u_{xx} + u_{yy}) = f(x,y), \quad 0 < x, \ y < 1 \tag{38}$$

$$u(x,y) = e^{\frac{x}{2a}} \sin(\pi y) \left(\frac{2e^{-\frac{1}{2a}} \sinh(\sigma x) + \sinh(\sigma(1-x))}{\sinh \sigma} \right) \tag{39}$$

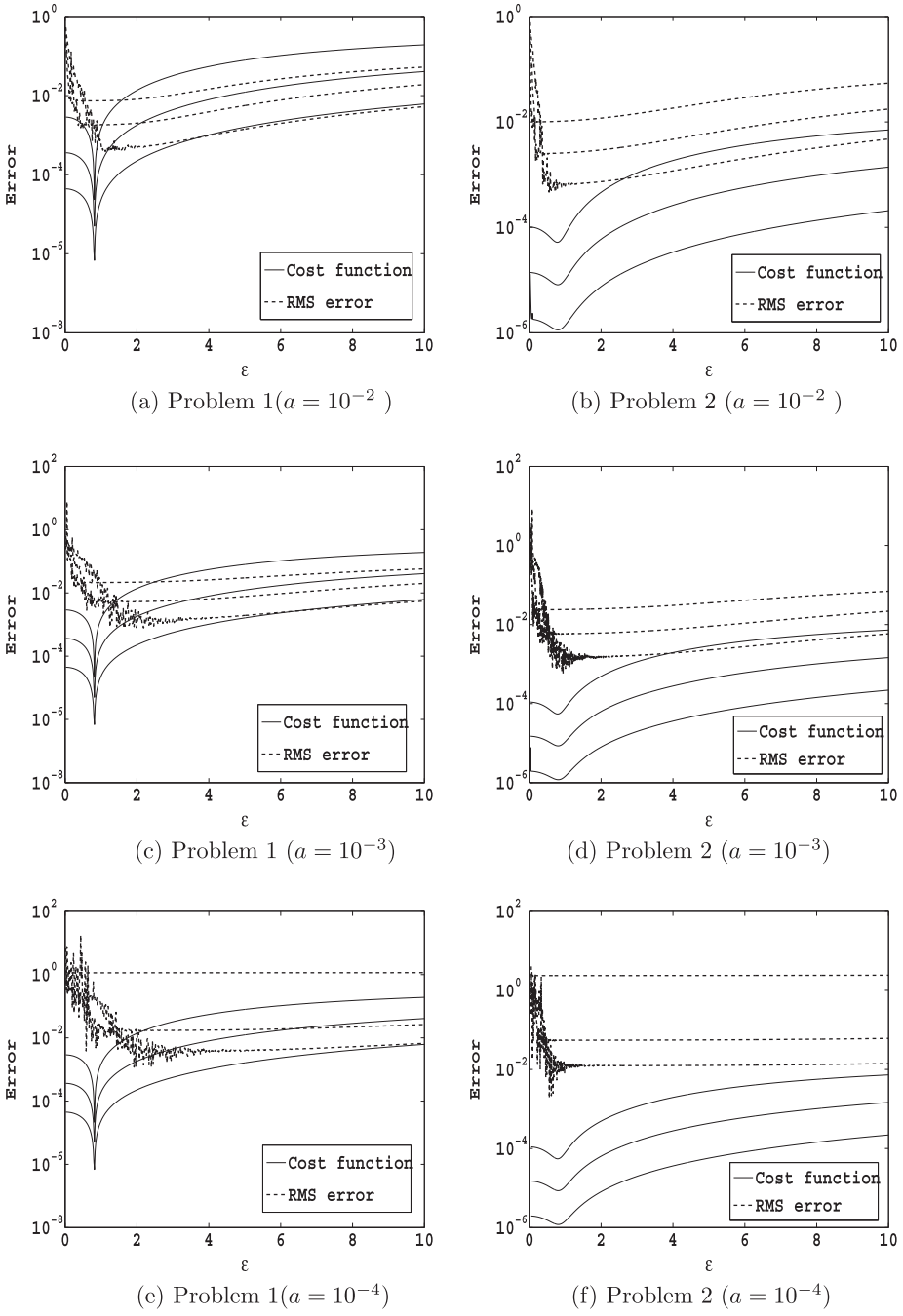

(a) Problem 1($a = 10^{-2}$) (b) Problem 2 ($a = 10^{-2}$)

(c) Problem 1 ($a = 10^{-3}$) (d) Problem 2 ($a = 10^{-3}$)

(e) Problem 1($a = 10^{-4}$) (f) Problem 2 ($a = 10^{-4}$)

Fig. 6. Comparison of RMS error & (*global*) Cost function against the Shape parameter for the Test problems 1 and 2, at $N = 41, 81, 161$ (from the top to bottom) over non-uniform points.

where $\sigma^2 = \pi^2 + 0.25a^{-2}$.

Test problem 4

$$u_x + u_y - a(u_{xx} + u_{yy}) = f(x,y), 0 < x,y < 1 \tag{40}$$

$$u(x,y) = e^{-(1-x)(1-y)/2a} \tag{41}$$

For the discretization of the domains of the chosen test problems, uniform, Chebyshev and two types of non-uniform [29] distribution of points are considered. A typical case of two-dimensional ($2D$) computational domain in $0 \leqslant x,y \leqslant 1$, with the chosen point distributions is presented in the Fig. 2. These points are generated using.

Table 3
Comparison of optimal shape parameters and the RMS errors calculated over the uniform, Chebyshev and the non-uniform points for the Test problem 1.

	$N \rightarrow$	Uniform points		Chebyshev points		Non-uniform points	
		81	161	81	161	81	161
$a = 10^{-2}$	Global	0.7661	0.7661	0.8176	0.8176	0.8176	0.8176
	RMS error	7.14(−3)	1.68(−3)	4.03(−3)	9.89(−4)	1.83(−3)	9.89(−4)
	Best	3.4966	3.501	0.1343	0.3843	0.8176	0.909
	RMS error	7.10(−3)	1.67(−3)	3.91(−3)	1.09(−3)	1.83(−3)	4.71(−4)
	Local	(5.4285, 11.4600)	(1.1369, 2.5124)	(0.12, 0.8118)	(0.4289, 2.9084)	(0.6624,1.1373)	(0.7360, 1.2639)
	RMS error	6.65(−3)	1.67(−3)	3.31(−3)	9.26(−4)	1.36(−3)	2.92(−4)
$a = 10^{-3}$	Global	0.7760	0.7760	0.8176	0.8176	0.8176	0.8176
	RMS error	1.17(−1)	4.76(−2)	2.85(−2)	5.66(−3)	5.43(−3)	2.80(−3)
	Best	(0, 50)	(0, 50)	0.1676	0.4010	0.8509	1.2510
	RMS error	1.17(−1)	4.76(−2)	2.31(−2)	1.44(−2)	3.94(−3)	2.59(−3)
	Local	(0.7860, 0.8107)	(0.7860, 1.0831)	(0.3662, 2.2537)	(0.3673, 1.500)	(0.6483, 2.1634)	(0.6964, 3.4399)
	RMS error	1.17(−1)	4.76(−2)	2.85(−2)	3.80(−3)	3.85(−3)	4.91(−4)
$a = 10^{-4}$	Global	0.801	0.801	0.8176	0.8176	0.8176	0.8176
	RMS error	4.78(−1)	2.14(−1)	3.11(+2)	8.85(−1)	3.91(−2)	3.34(−2)
	Best	(0, 50)	(0, 50)	0.1177	0.8009	0.8509	1.917
	RMS error	4.78(−1)	2.14(−1)	1.58	6.40(−1)	1.494(−2)	7.92(−3)
	Local	(0.8102, 1.010)	(0.8298, 1.0373)	(0.01, 0.8447)	(0.2118, 0.8354)	(0.8313, 1.8686)	(0.5114, 2.1113)
	RMS error	4.78(−1)	2.14(−1)	3.33(−2)	3.76(−3)	6.67(−3)	1.01(−3)

Table 4
Comparison of optimal shape parameters and the RMS errors calculated over the uniform, Chebyshev and the non-uniform points for the Test problem 2.

	$N \rightarrow$	Uniform points		Chebyshev points		Non-uniform points	
		81	161	81	161	81	161
$a = 10^{-2}$	Global	0.5821	0.5948	0.6407	0.6341	0.8103	0.8103
	RMS error	4.87(−3)	1.19(−3)	4.67(−3)	1.17(−3)	1.55(−3)	3.89(−4)
	Best	0.3587	0.4149	0.1548	0.2480	0.1773	0.7264
	RMS error	4.86(−3)	1.19(−3)	4.48(−3)	1.37(−3)	1.58(−3)	3.89(−4)
	Local	(0.0010, 4.9048)	(0.6765, 6.6094)	(0.1250, 7.1465)	(0.3493, 15.4545)	(0.0038, 3.4044)	(0.2723, 6.2708)
	RMS error	4.63(−3)	1.19(−3)	3.88(−3)	9.95(−4)	1.50(−3)	3.85(−4)
$a = 10^{-3}$	Global	0.5948	0.6346	0.6607	0.6407	0.8304	0.8083
	RMS error	1.36(−1)	4.25(−2)	2.98(−2)	5.70(−3)	5.50(−3)	1.44(−3)
	Best	(0, 50)	(0, 50)	0.1614	0.3412	0.3035	0.9414
	RMS error	1.36(−1)	4.25(−2)	2.48(−2)	1.20(−2)	9.12(−3)	1.80(−3)
	Local	(0.1022, 4.1568)	(0.1022, 5.9024)	(0.1240, 26.9759)	(0.3176, 390.567)	(0.4980, 2.7375)	(0.8522, 3.9433)
	RMS error	1.36(−1)	4.25(−2)	2.10(−2)	4.83(−3)	4.71(−3)	6.78(−4)
$a = 10^{-4}$	Global	0.6497	0.5926	0.6532	0.6470	0.8087	0.8087
	RMS error	6.39(−1)	2.95(−1)	8.18(+2)	9.24(−2)	5.51(−2)	1.29(−2)
	Best	1.0	1.0	0.1682	0.5040	0.3050	0.5599
	RMS error	6.39(−1)	2.95(−1)	2.09	1.32(−1)	4.22(−2)	5.13(−3)
	Local	(0.1022, 4.1568)	(0.1022, 4.8596)	(0.002, 1.5009)	(0.0460, 41.921)	(0.2639, 3.500)	(0.8276, 3.8832)
	RMS error	6.39(−1)	2.95(−1)	6.58(−1)	3.75(−2)	4.90(−2)	2.08(−3)

- Chebyshev points

$$x_i = \frac{1}{2}\left[1 - \cos\left(\frac{i-1}{N_x - 1}.\,\pi\right)\right], \quad i = 1, 2, \ldots, N_x \tag{42}$$

$$y_j = \frac{1}{2}\left[1 - \cos\left(\frac{j-1}{N_y - 1}.\,\pi\right)\right], \quad j = 1, 2, \ldots, N_y \tag{43}$$

- Non-uniform points (I),

$$x_i = \frac{i-1}{Nx - 1} + \frac{\zeta}{\pi}\sin\left(\frac{i-1}{Nx - 1}.\pi\right), \quad i = 1, 2, \ldots, Nx \tag{44}$$

$$y_j = \frac{j-1}{Ny - 1}, \quad j = 1, 2, \ldots, Ny \tag{45}$$

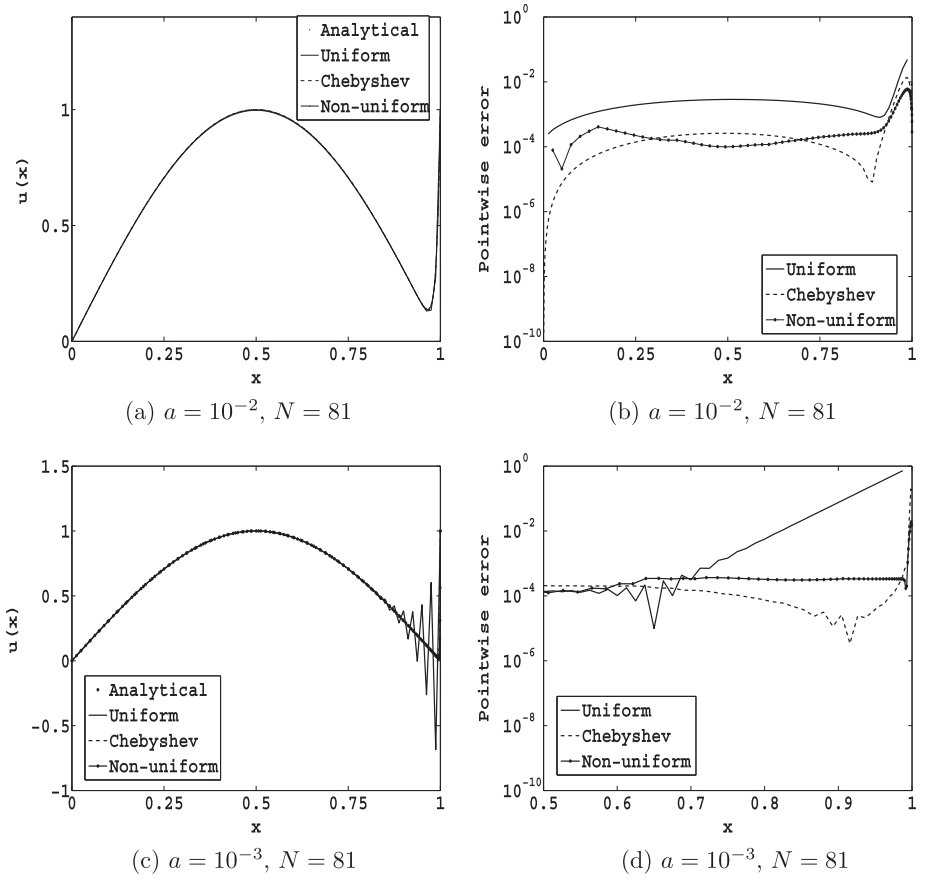

Fig. 7. Comparison of analytical & numerical solutions and point wise errors, for the Test problem 1.

- Non-uniform points (II)

$$x_i = \frac{i-1}{Nx-1} + \frac{\zeta}{\pi}\sin\left(\frac{i-1}{Nx-1}.\pi\right), \quad i = 1,2,\ldots,Nx \tag{46}$$

$$y_j = \frac{j-1}{Ny-1} + \frac{\eta}{\pi}\sin\left(\frac{j-1}{Ny-1}.\pi\right), \quad j = 1,2,\ldots,Ny \tag{47}$$

where N_x, N_y are the number of points in the x, y directions respectively, ζ and η $(0 \leqslant \zeta, \eta < 1)$ are the stretching parameters used to control the point density. That is, with $\zeta = \eta = 0$, these formulae generate uniform distribution of points. In all the numerical experiments carried out in this work, the values of ζ and η are fixed as 0.8 when the diffusion parameter is 10^{-2} and it is raised to 0.95 for all the other smaller values of a. Point wise errors are compared, to study the performance of the developed algorithm over different nodal distributions. The point wise errors are calculated using

$$\text{Pointwise error } (i) = |U_i - u_i|, \quad i = 1,2,\ldots,N \tag{48}$$

where U is the analytical solution, u is the numerical solution and N is the total number of points in the computational domain. While computing the (near) optimal shape parameter, the number of centers in the local support domain is fixed as $n_i = 4$ for one dimension and $n_i = 7$ for two dimensional problems. However, while solving the CDE, the number of centers in the local support domain is fixed as $3, 5$ for one and two dimensional problems, respectively. The final algebraic systems are solved using BiCGstab solver.

5.1. One dimensional problems

The developed scheme is first applied on the Test problem 1 with Gaussian and also with multiquadric and the corresponding RMS errors are compared in Tables 1 and 2 with number of centers 41 and 161, respectively. These comparisons show that both RBFs produce similar solutions, therefore, the rest of the computations are carried out with multiquadric.

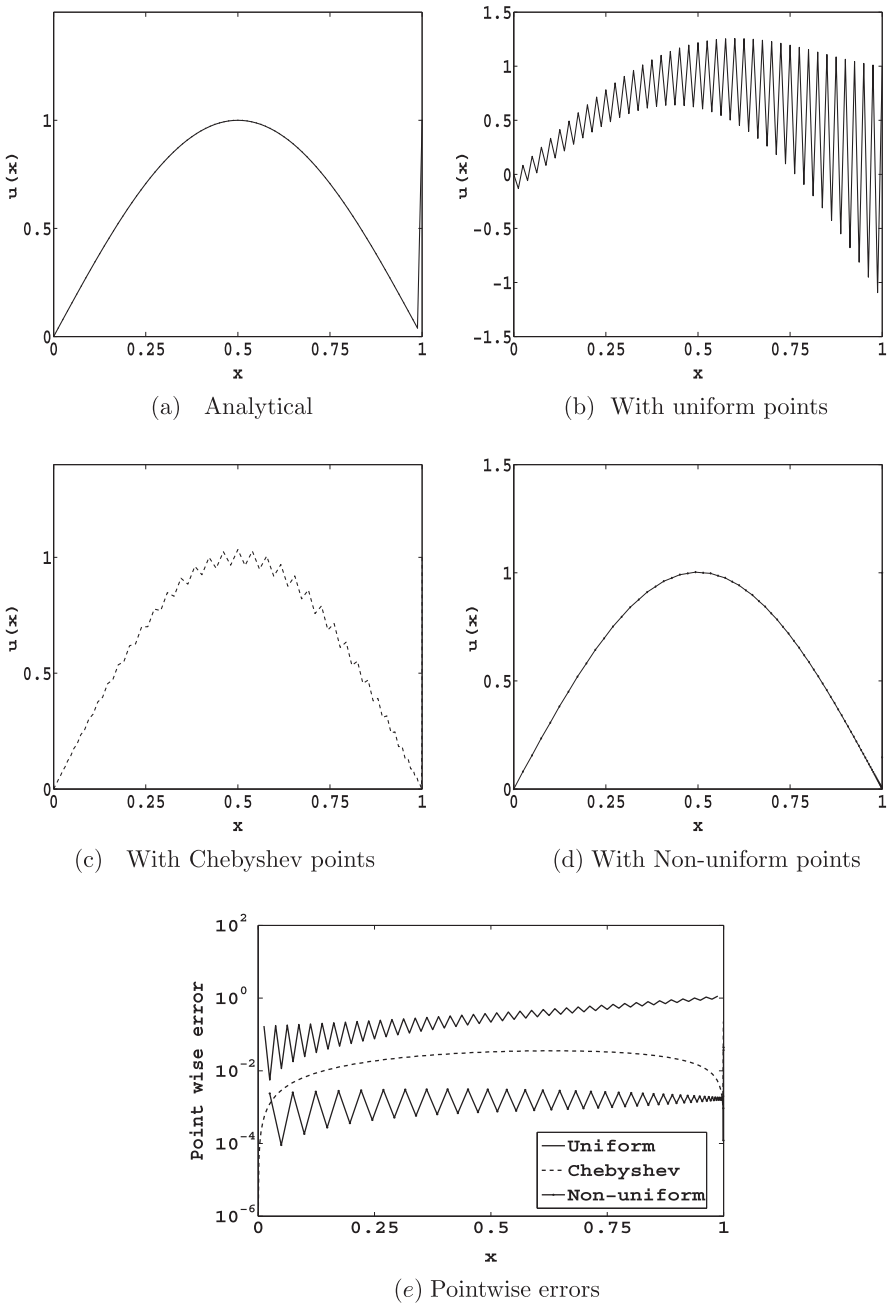

Fig. 8. Comparison of analytical & numerical solutions and point wise errors, for the Test problem 1, at $a = 10^{-4}, N = 81$.

In order to study the correlation between the (RMS) error function and the (global) Cost function for the convection dominated problems, test problems 1 and 2 are solved over uniform, Chebyshev and a non-uniform distribution of the points, in a fixed interval of the shape parameter. The number of points is varied as $N = 41, 81$ and 161, with the diffusion parameter changing from $a = 10^{-2}, 10^{-3}$ and to 10^{-4} and the corresponding error curves have been compared in the Figs. 4–6. In the Fig. 4, the comparisons over uniform distribution of points $N = 41$, 81 and 161 are demonstrated. It is clear from this figure that the (global) Cost function and the error function are following a similar pattern. Therefore, cost function can be minimized, particularly for $a = 10^{-2}$ due to its variation with respect to ε, instead of error function since the latter can't be computed unless the exact solution of the problem is known. In Figs. 5 and 6, the cost and error functions are compared for one dimensional problems over Chebyshev and non-uniform points, respectively. It is clear from the Fig. 5 that, both error and Cost functions have their global minima in almost same interval for all the chosen cases. If the points are non-uniform, it can

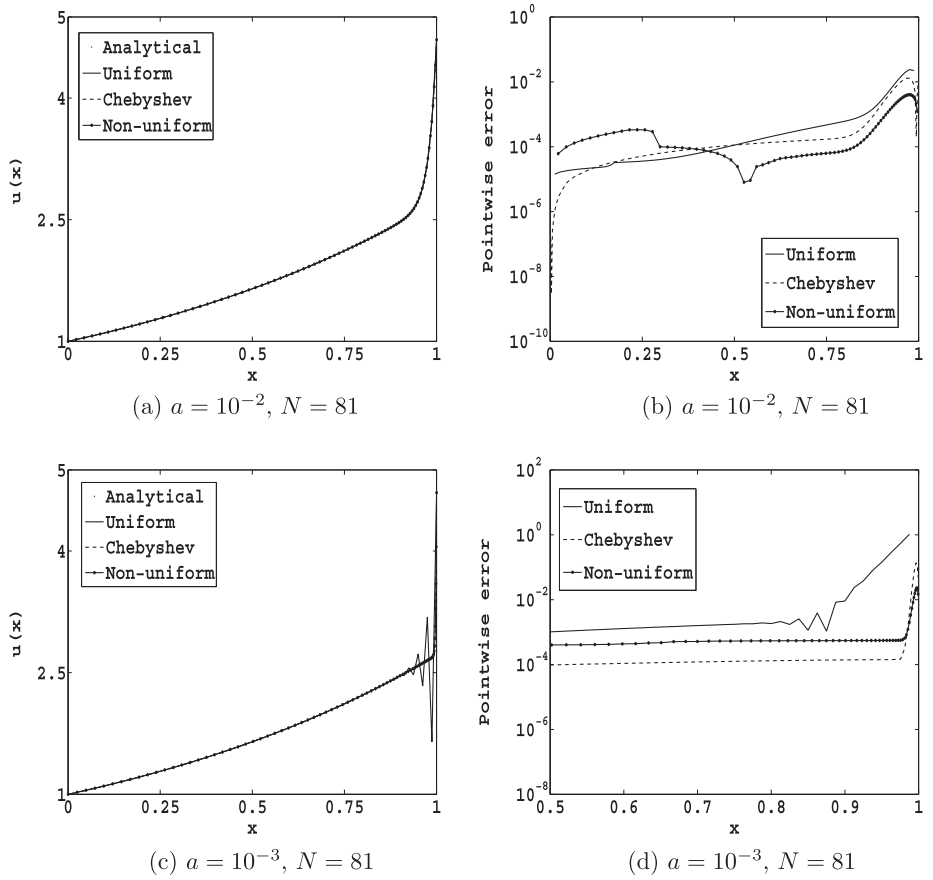

Fig. 9. Comparison of analytical & numerical solutions and point wise errors, for the Test problem 2.

be observed from the Fig. 6 that, the error and Cost functions are having a very good agrement when compared with the other two cases. Therefore, optimizing the cost function computed over the chosen non-uniform point distribution must give the best possible solution.

The one dimensional test problems are also solved with variable shape parameter and the RMS errors have been compared in Tables 3 and 4 for problems 1 and 2, respectively. The RMS errors obtained with the global optimum shape parameter (referred as Global), best shape parameter (referred as Best) and local variable shape parameter (referred as Local) are compared in these tables for the diffusion parameter $10^{-2}, 10^{-3}, 10^{-4}$. The best shape parameter is the value of the shape parameter at which the RMS curves have a global minimum with in the chosen range of the shape parameter. The number of centers is varied as 81 and 161 and the computations are carried out over uniform, Chebyshev and non-uniform distribution of centers. Since the local shape parameter is a variable unlike the other two, its minimum and maximum values are reported in the tables for all the chosen cases. It is clear from these comparisons that the results obtained with variable shape parameter are better than the other two for all the chosen cases. These comparisons also reveal that for the convection dominated problems, the non-uniform distribution of points is giving the best solution and then the Chebyshev points for both 81 and 161 centers. Further, the accuracy of the solutions obtained over these two distributions have improved by an order when 161 centers are used, however, the same is not seen with uniform points. To highlight the accuracy of solutions with different point distributions, the solutions and their RMS errors are compared in Figs. 7–14. For the sack of comparison, the analytical solutions are also included in these figures.

It is clear from Figs. 7 and 9 that, when the diffusion parameter a is 10^{-2}, the numerical solutions are non-oscillatory, however when a is reduced to 10^{-3}, the solutions are started becoming oscillatory particularly over the uniform points. If a is further reduced to 10^{-4}, Figs. 8 and 10 show that the solutions over Chebyshev points are also marginally oscillatory but the amplitude of these oscillations is much less than the corresponding uniform case. The results with non-uniform points are remained non-oscillatory and better than the other two cases. The oscillations with uniform points are anyway anticipated but the interesting observation is the oscillations with Chebyshev points. The RMS-error comparisons reported in these plots also confirm that the solutions obtained using non-uniform point distributions are best among the chosen three point distributions. It is also clear from these figures that, near the boundary layer, the magnitude of the point wise error obtained over the uniform points is much more when compared to the point wise errors obtained over the Chebyshev

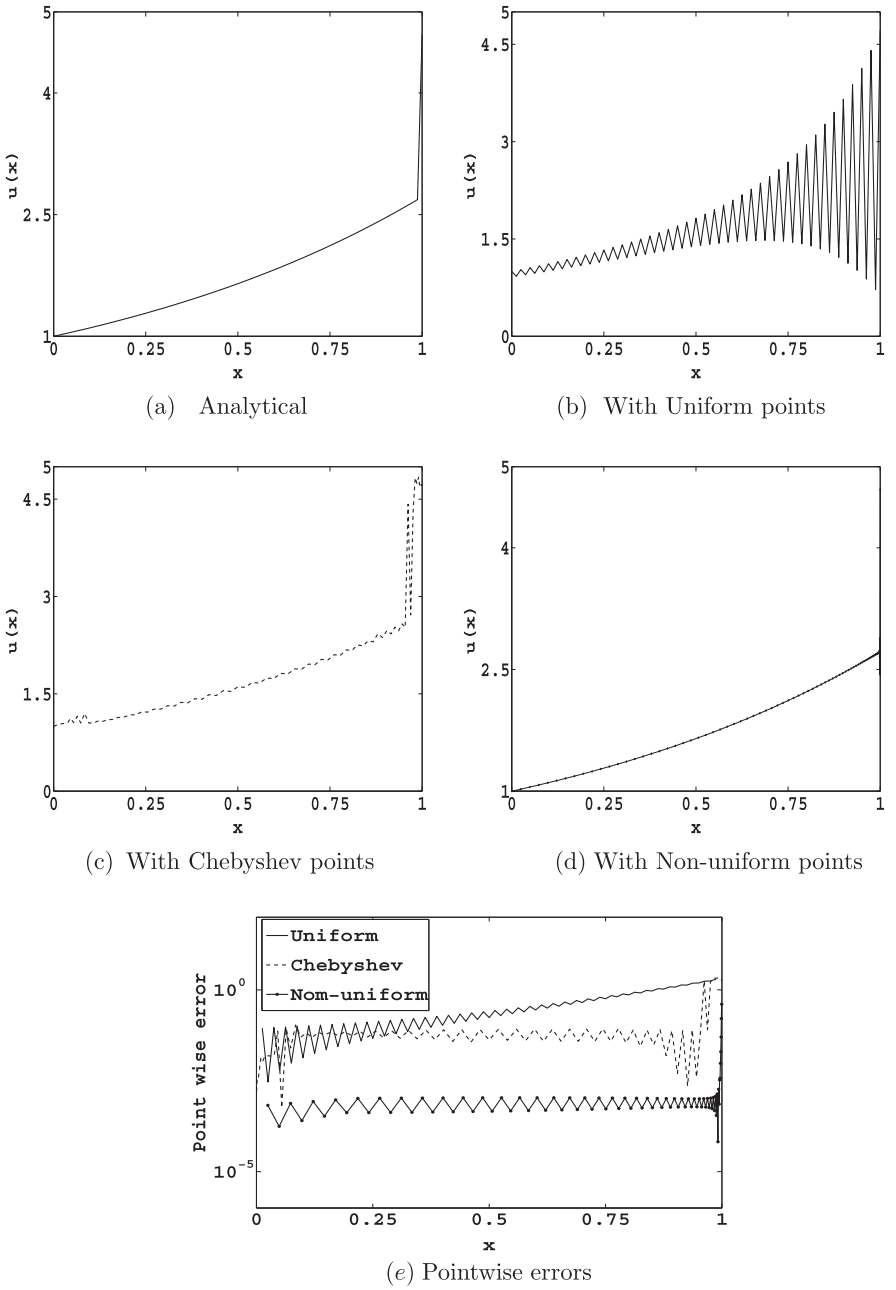

Fig. 10. Comparison of analytical & numerical solutions and point wise errors, for the Test problem 2, at $a = 10^{-4}, N = 81$.

as well as the non-uniform points. These oscillations are disappeared when the problems are solved over the non-uniform points, with the same number of points ($N = 81$). Also, looking at the Figs. 8(e) and 10(e), near the boundary layer, the point wise errors obtained over the non-uniform points are less than the point wise errors over the uniform and the Chebyshev points.

To understand the improvement in the accuracy, the test problems are also solved with $N = 161$ centers and the corresponding solutions and the point wise errors are reported in the Figs. 11–14. The results for $a = 10^{-2}$ and $a = 10^{-3}$ are shown in Figs. 11 and 13 while results for $a = 10^{-4}$ are shown in Figs. 12 and 14. For the case with $a = 10^{-4}$, the numerical solutions obtained over the uniform points are still oscillatory and the improvement is marginal, however, for the other two cases, the accuracy is improved by an order. One safe conclusion one can make with these observations is for the convection dominated problems, the LRBF scheme with the local optimal shape parameter applied over the non-uniform points produces more

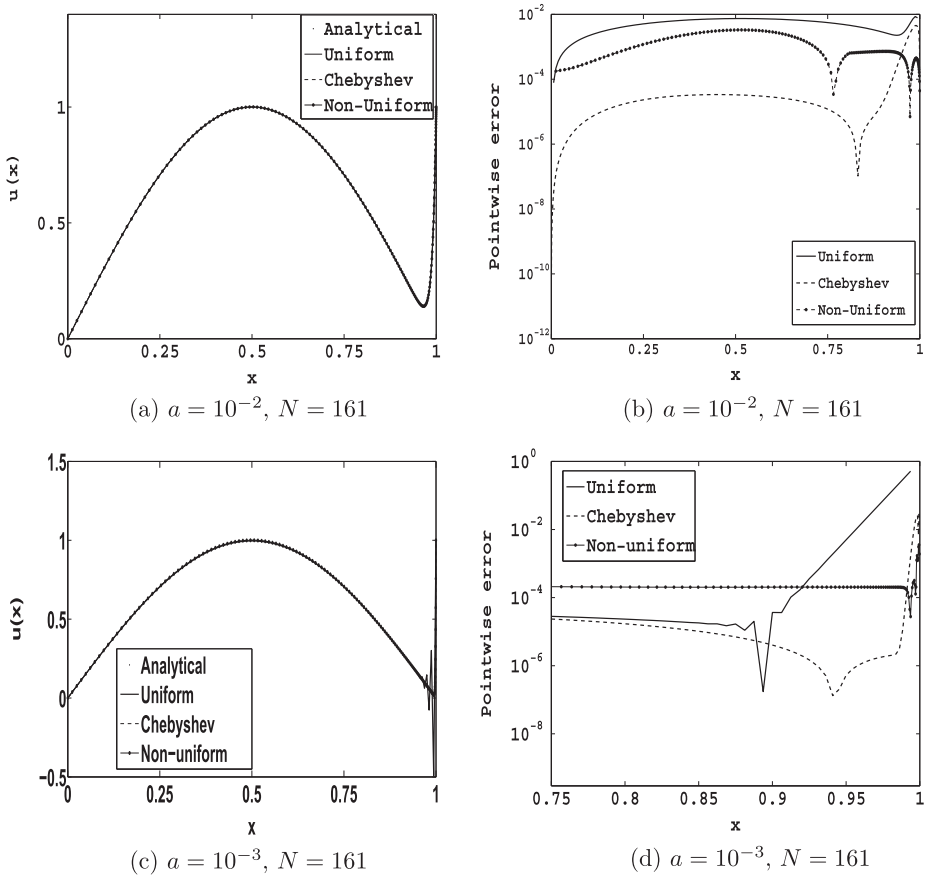

(a) $a = 10^{-2}$, $N = 161$ (b) $a = 10^{-2}$, $N = 161$

(c) $a = 10^{-3}$, $N = 161$ (d) $a = 10^{-3}$, $N = 161$

Fig. 11. Comparison of analytical & numerical solutions and point wise errors, for the Test problem 1.

accurate and stable results, with the minimum number of points. Further, observing the comparisons of the point wise errors of these three point distributions, for all *a*, the solutions obtained over Chebyshev points are initially (in the smooth regions of the domain) are more accurate when compared with the other two followed by the results with uniform case. However, once the region of interest comes close to the boundary layer, slowly, the errors in these solutions grow, and the solutions with non-uniform points becomes better. This is the trend generally observed for all *a* and for all *N*. This peculiar behavior can be attributed to the distribution of the points in each of these cases. Since the point distribution in Chebyshev points is finer in the ends and coarser in the center, the accuracy, at the end region (non-layer end of the region because in the layer region, the points with non-uniform is more finer), with these points is expected to be better over the other two. The second best, in terms of the finer points in non-layer regions, is the uniform points, therefore the same is faring better over the non-uniform points. That is the fineness of the points in non-uniform distribution is obtained at the cost of the smooth region however, this is not a big draw back because the growth in the errors for uniform and Chebyshev are such that if we compare the mean errors (over the whole domain) of the three cases, the RMS error obtained with non-uniform points is much less than the other two.

The comparisons, through figures and tables, made until now brought out the effect of distribution of points on the accuracy of the solutions, however to highlight the effect of the shape parameter on the accuracy, one should compare the results with the corresponding results obtained with a constant shape parameter. To realize this, the RMS errors (variable), previously presented in Tables 3 and 4 for problems 1 and 2, respectively, are now compared with the corresponding error norms obtained with some constant shape parameters. Looking at the variation of global cost function presented in the Figs. 4–6 (for $\varepsilon > 2$, the cost function in these figures is more or less a straight line, showing a possibility of minimum error only for $\varepsilon < 2$), the shape parameter is fixed as 1.0, 0.5, 0.1, 0.05 and the corresponding errors (mean and max) are obtained and compared in Table 5. For the sake of comparison, the values with variable shape parameter are also included in this table. It is clear from this comparison that, the results obtained with variable shape parameter, particularly with Chebyshev and non-uniform points, are better than with the constant shape parameter. The improvement is substantial with the Chebishev points but not felt much with the unform points. This is an expected behavior, because there is hardly any variation in the global cost function plotted in Fig. 4 for uniform points.

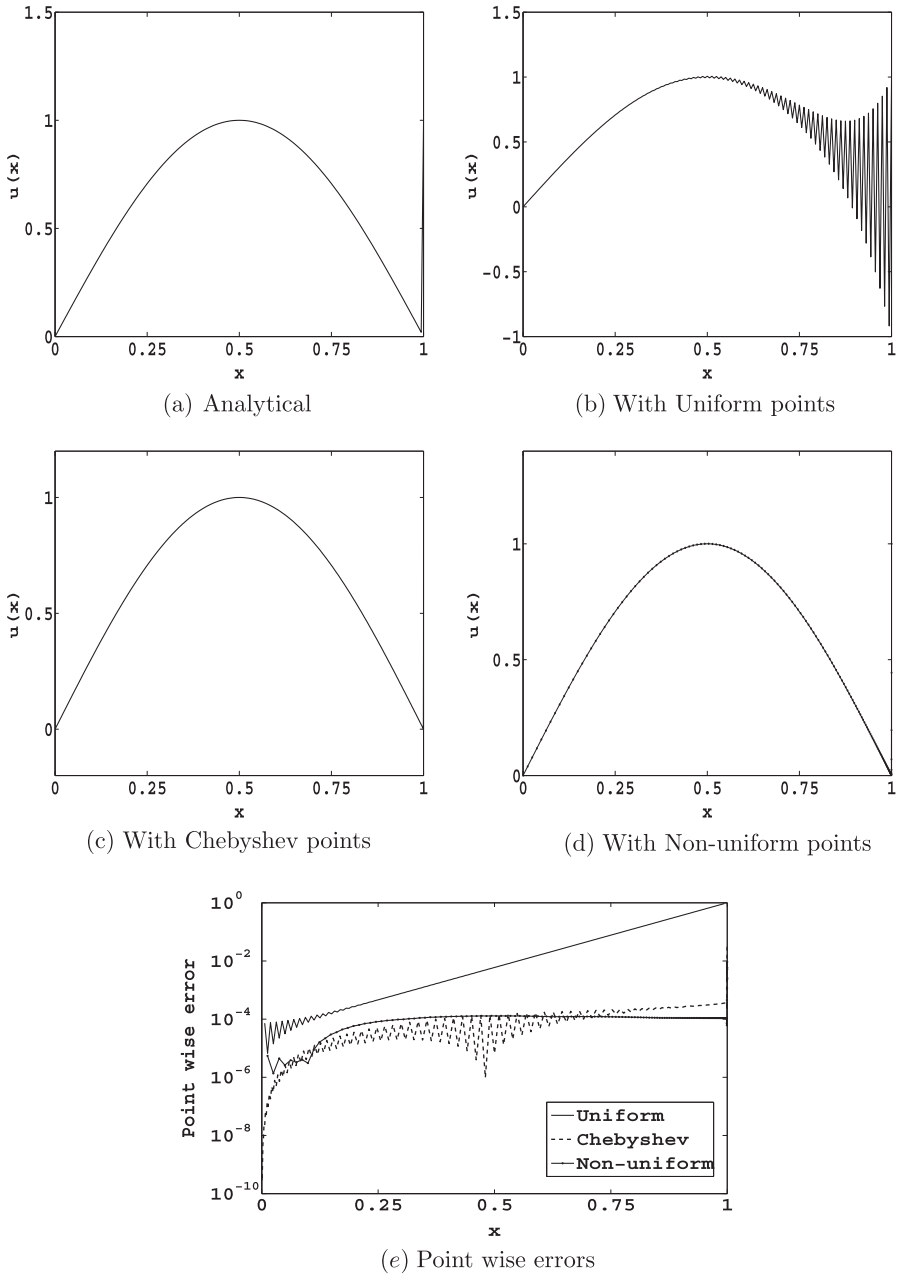

Fig. 12. Comparison of analytical & numerical solutions and point wise errors, for the Test problem 1, at $a = 10^{-4}, N = 161$.

5.2. Two dimensional problems

It is clear from the earlier section that the LRBF scheme with a variable shape parameter, obtained using (29), has produced the most accurate results. Therefore, the two dimensional test problems have been solved using the LRBF scheme with a variable shape parameter. Test problem 3 has been taken from Gartland [30]. This problem represents a convection dominated flow, for small values of a. The analytical solution of this problem has a steep boundary layer along the edge $x = 1$, and shear layers along the top and bottom edges, that is, at $y = 0$ and $y = 1$. The number of centers, $Nx \times Ny = 81 \times 81$, is fixed to find the numerical solutions over the uniform, Chebyshev and the non-uniform (I) distribution of the points, for various diffusion parameters, $a = 10^{-2}, 10^{-3}$ and 10^{-4}. The obtained numerical solutions over the chosen three point distributions are compared with the corresponding analytical solutions in Figs. 15–17 for the diffusion parameters $a = 10^{-2}, 10^{-3}$ and 10^{-4}, respectively. The comparison of surface plots, u is constant contours and point wise errors along $y = 0.5$ (center line) with

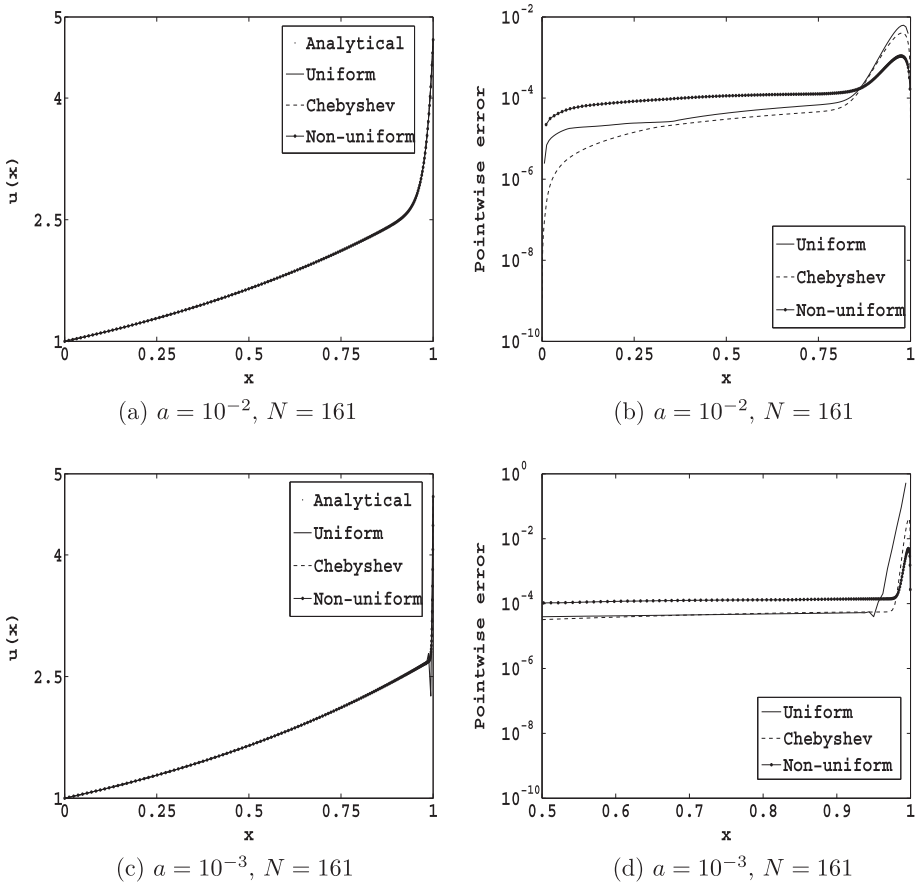

Fig. 13. Comparison of analytical & numerical solutions and point wise errors, for the Test problem 2.

the three point distributions are included in these figures. The comparison of surface and contour plots in Fig. 15 at $a = 10^{-2}$ confirm that all the three numerical solutions are close to the analytical solution at this diffusion parameter. The comparison of point wise errors at the y center line also confirms the pattern which has been observed for one dimensional problems. That is, in the smooth regions (close to $x = 0$ in this example), the solution obtained with Chebyshev points is most accurate followed by the solution obtained with uniform points. However, the errors in these solutions have gradually increased if the region of observation is moved towards the boundary layer ($x = 1$ in this example). On the other hand, the solutions obtained with non-uniform points maintained a uniform accuracy through out the region and their mean error is also smaller than the corresponding mean errors of the solutions obtained with uniform and Chebyshev points.

When the diffusion parameter a is reduced to 10^{-3}, as shown in Fig. 16, the surface and the contour plots near $x = 1$ for the uniform case (subplot 16b) show some deviation from the analytical solution however the solutions presented with Chebyshev and non-uniform points are still close to the corresponding analytical solution. The comparison of the point wise errors, shown in this figure, unveils that the solution obtained with uniform points started with a better accuracy when compared with the other two, however once x crosses 0.25, the errors in this solution sharply increased and became very inaccurate near $x = 1$. The Chebyshev solution still maintained a reasonable accuracy and became oscillatory only in the region which is very close to $x = 1$. The Non-uniform solution maintained a uniform accuracy and once again the best in terms of mean error when compared with the other two. Finally, when the diffusion parameter a is further reduced to 10^{-4}, as shown in Fig. 17, the solutions with uniform and Chebyshev points became inaccurate, but the non-uniform solution preserved its supremacy over the other two by producing stable solutions. As shown in the figure, the Chebyshev solution particularly oscillated in the range -20 to 10 making the scheme completely unstable. The solution with uniform points, though with in the range of -1 to 2, it is failed to capture the sharp raise in the solution near $x = 1$ but produced a smooth solution. In this case, the u = constant contours also deviated substantially from the corresponding analytical solution. The comparison of point wise errors presented in this figure also confirms that the solution obtained with non-uniform points is the best through out the region from $x = 0$ to 1 though it has small oscillations in the range of 10^{-3} to 10^{-4}. Similar oscillations are also visible with uniform case but in the range 10^{-2} to 10^{-1} near $x = 0$ and raises to order one near $x = 1$. The solution with Chebyshev points is much above these points (errors are of order one form $x = 0$ itself) and a huge kink can be seen

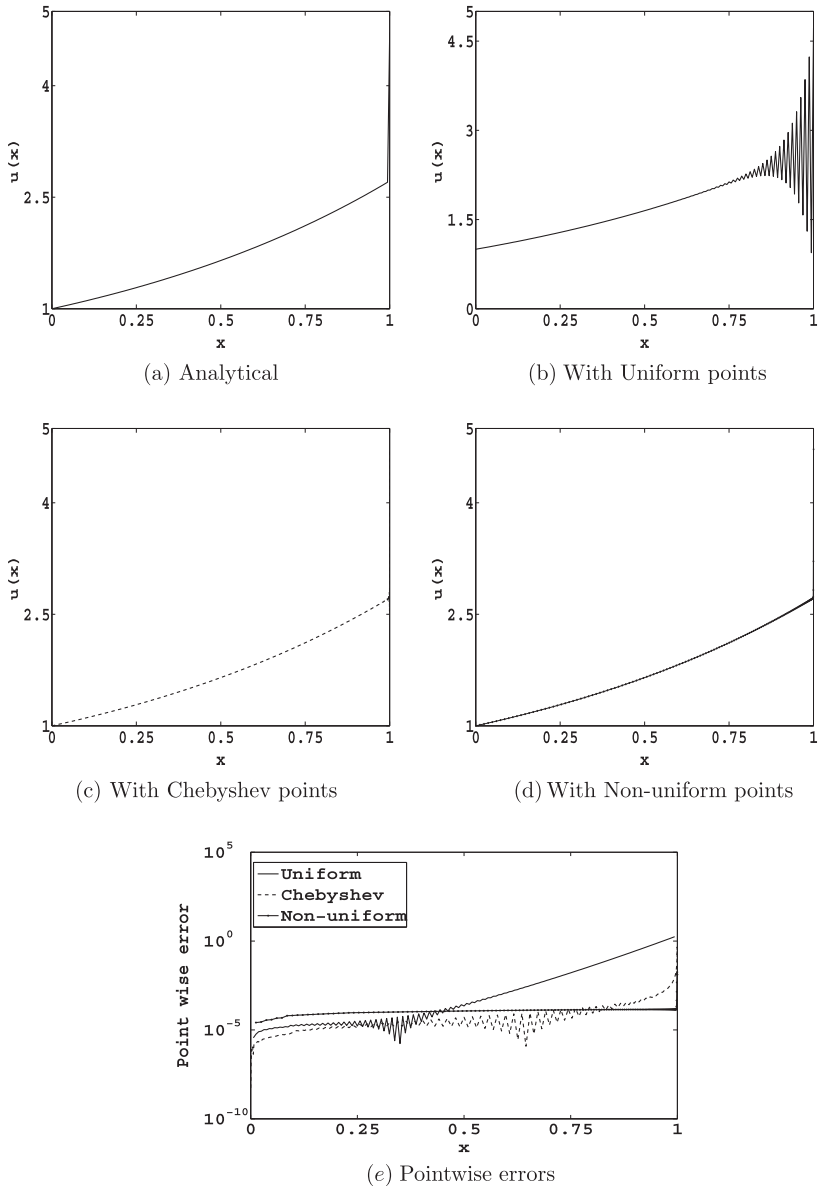

Fig. 14. Comparison of analytical & numerical solutions and the corresponding point wise errors, for the Test problem 2, at $a = 10^{-4}, N = 161$.

Table 5
Comparison of maximum and RMS errors computed with a fixed shape parameter at $a = 10^{-4}, N = 81$.

	ε	Uniform points		Chebyshev points		Non-uniform points	
		RMS error	Max error	RMS error	Max error	RMS error	Max error
Test problem 1	0.05	4.71(−1)	1.12	5.62	9.23	3.95(−1)	1.17
	0.1	4.78(−1)	1.13	4.19	6.90	2.01	9.70
	0.5	4.78(−1)	1.13	3.31(+2)	5.42(+2)	2.87	2.21(+1)
	1.0	4.78(−1)	1.13	3.11(+2)	5.09(+2)	1.72(−2)	1.52(−1)
	ε_{var}	4.78(−1)	1.13	3.33(−2)	2.26(−1)	6.67(−2)	4.38(−2)
Test problem 2	0.05	6.34(−1)	1.96	2.12	3.38	9.65	1.63(+1)
	0.1	6.39(−1)	1.96	2.16	3.45	4.52(−1)	2.01
	0.5	6.39(−1)	1.96	7.12(+2)	1.13(+3)	5.44(−2)	4.80(−1)
	1.0	6.39(−1)	1.96	1.02(+3)	1.63(+3)	5.50(−2)	4.86(−1)
	ε_{var}	6.39(−1)	1.96	6.58(−1)	2.16	4.90(−2)	4.03(−1)

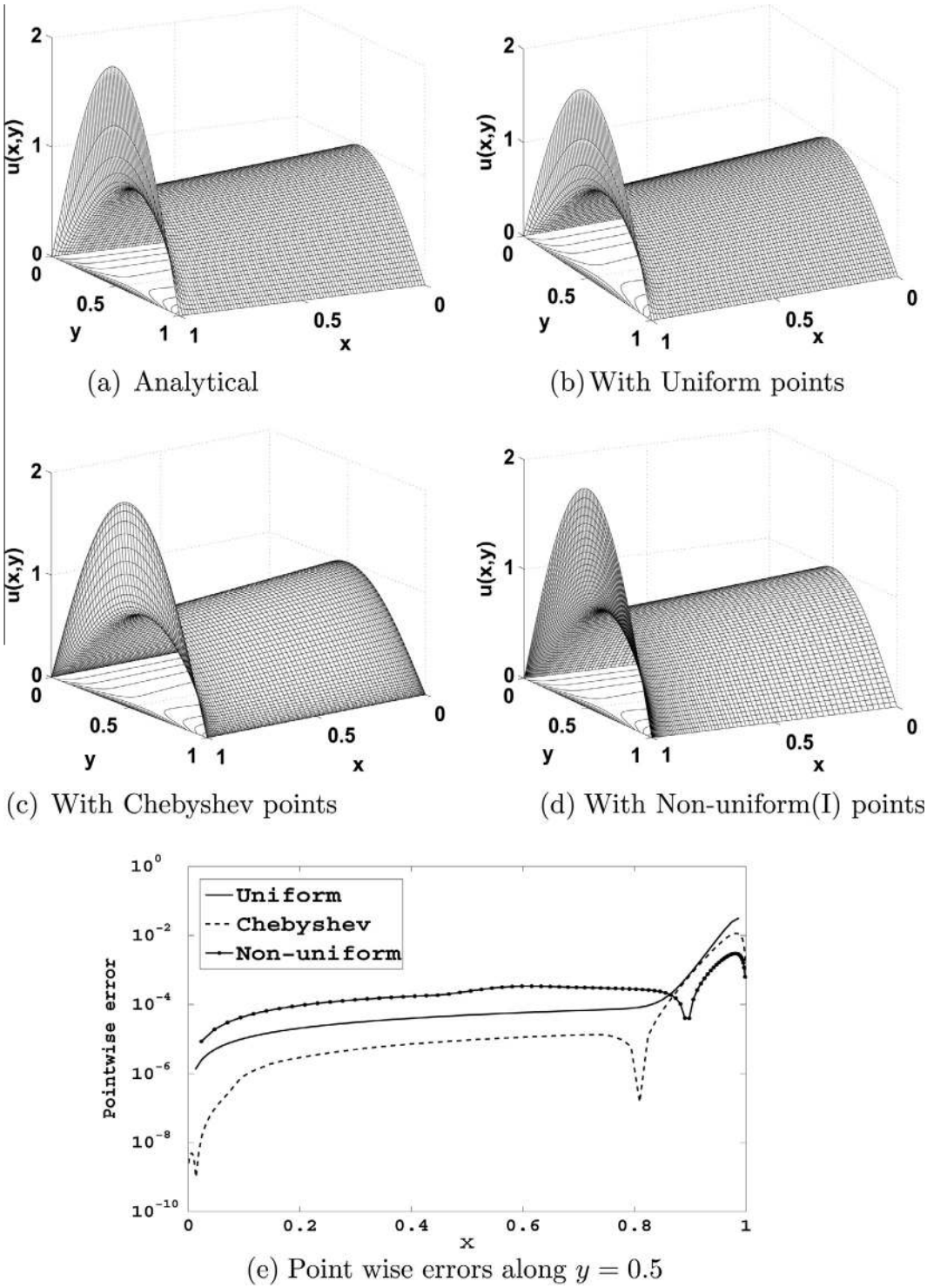

Fig. 15. Comparison of analytical and numerical solutions and point wise errors along $y = 0.5$ for the Test problem 3, at $a = 10^{-2}$ with 81×81.

clearly near $x = 0.7$ revealing the unstable nature of the solution. For the sack of quantitative comparison, the minimum and the maximum values of the variable shape parameter and the corresponding RMS and the maximum error norms are reported in the Table 6. Interestingly, the variation in the shape parameter has followed a similar pattern for all the three point distributions at $a = 10^{-2}$, but the same is not true for smaller values of a. It is found that the minimum and maximum values

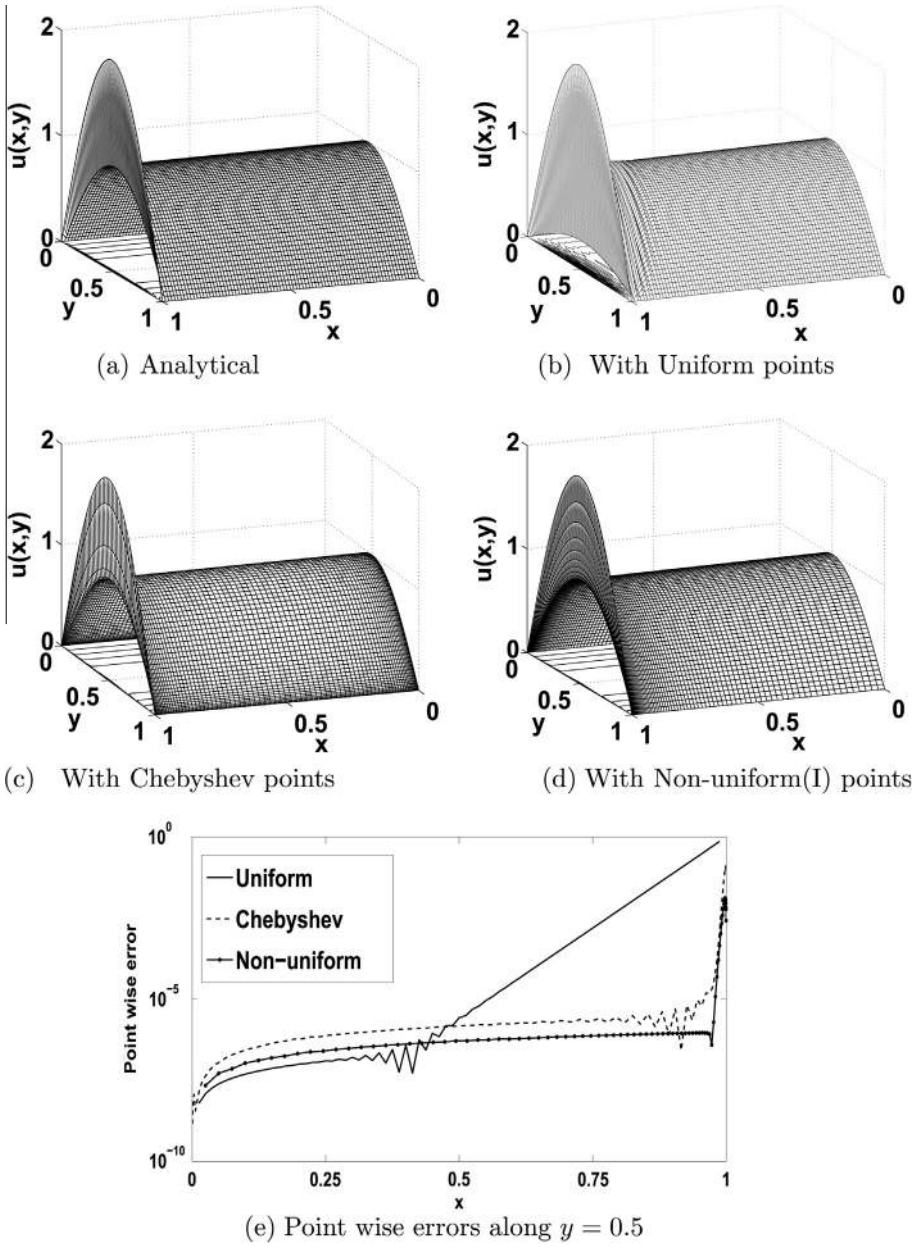

Fig. 16. Comparison of analytical and numerical solutions and point wise errors along $y = 0.5$ for the Test problem 3, at $a = 10^{-3}$ with 81×81.

have no such similarity between the three cases. The mean error with uniform points is started with 10^{-3} at $a = 10^{-2}$ but dropped to 10^{-1} when a is reduced to 10^{-4}. The trend in the case of Chebyshev points is also similar except that the maximum error is very large at $a = 10^{-4}$. The mean errors with non-uniform points are the smallest and the drop in the accuracy, when a is reduced to $a = 10^{-4}$ is only one order and still maintained at 10^{-3}. The maximum errors are also very satisfactory in this case.

The test problem 4, has two-sided boundary layer near the edges $x = 1$ and $y = 1$. Once again, the numerical solutions have been obtained over the uniform, Chebyshev and the non-uniform (II) distribution of points for different values of the diffusion parameter, $a = 10^{-2}, 10^{-3}$ and 10^{-4} with number of centers, $Nx \times Ny = 81 \times 81$. First to give an overview of the performance of the scheme at the chosen diffusion parameters, the point wise errors along $y = 0.95$ for $a = 10^{-2}$ and $a = 10^{-3}$ and $y = 0.25, .5, .75, .95$ for $a = 10^{-4}$ are presented in the Fig. 18. Instead of center line, in the first two cases, the point wise errors are presented at $y = 0.95$, because due to the double sided boundary layer in this problem, the accuracy in the region close to $x = 1$ or $y = 1$ may be effected more when compared with other regions. However, for $a = 10^{-4}$, point wise errors are presented at four distinct lines distributed through out the domain.

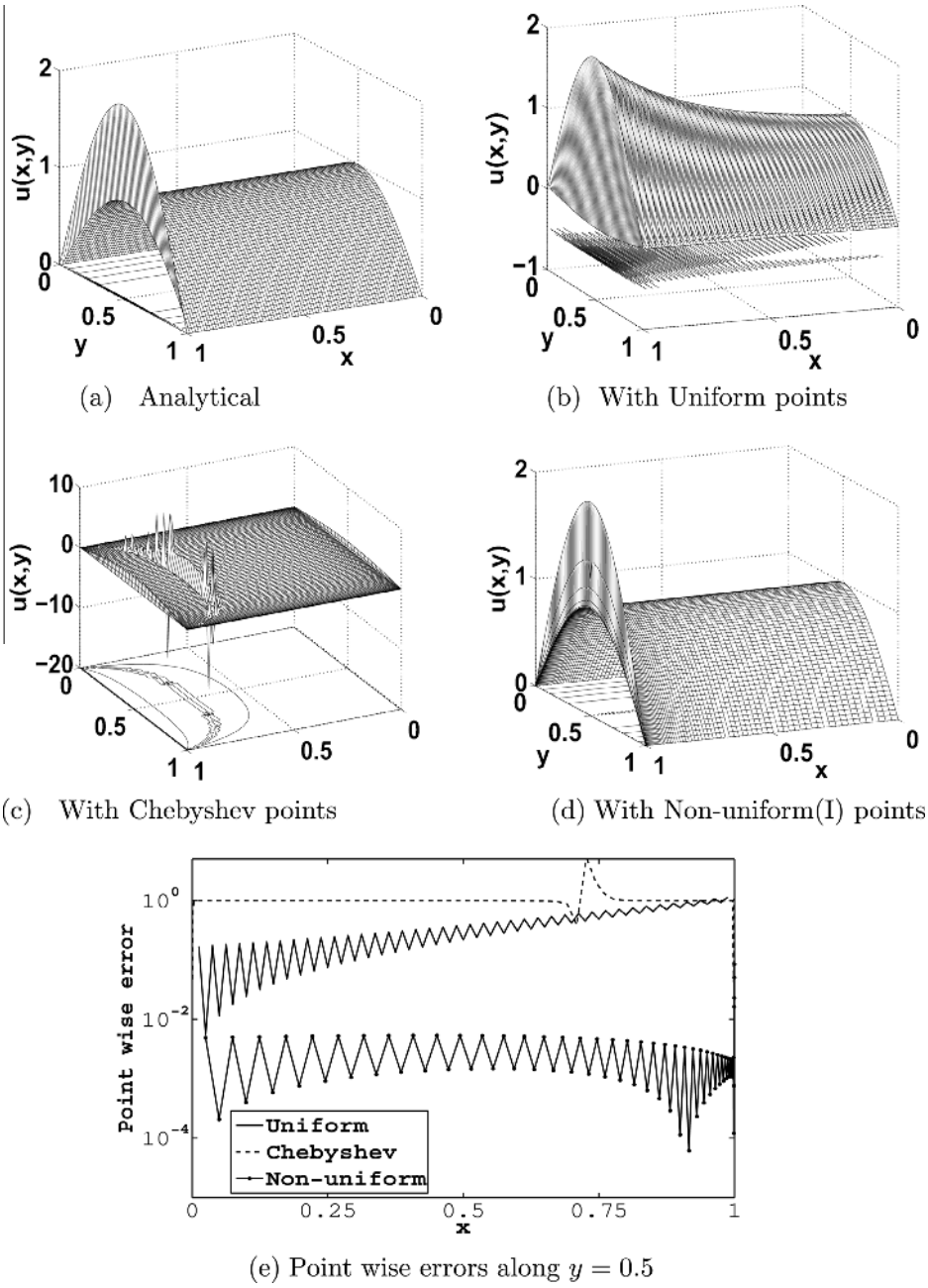

Fig. 17. Comparison of analytical and numerical solutions and point wise errors along $y = 0.5$ for the Test problem 3, at $a = 10^{-4}$ with 81×81.

As expected, at $a = 10^{-2}$, the three error plots are almost similar to what was observed for the earlier problem except that the solution with Chebychev points is slightly inferior when compared with the other two but very much with in the tolerance limits. This is also clear from the Fig. 19 wherein the analytical and numerical solutions are compared for this diffusion parameter. When the diffusion parameter is reduced to $a = 10^{-3}$ initially (in the smooth region) the Chebyshev and nonuniform solutions became very accurate but the errors with the former scheme increased suddenly in a very narrow region and then stabilized in the remaining part of the domain. For the latter case, though there is an increase in the error through out the domain but it was steady and also less than the other two. The point wise errors with uniform points is high when compared with the other two and the same is also can be seen in the Fig. 20 wherein the analytical and numerical solutions are compared for this diffusion parameter. When the solution with the nonuniform points imitated nicely the analytical solution, the other two show some deviation, particularly in the boundary layer region. To highlight the magnitude of deviation, the point wise error plots for the entire region for the chosen three point distributions

Table 6
Comparison of RMS and maximum errors computed with a variable shape parameter for the Test problem 3 & 4, at $N_x \times Ny = 81 \times 81$.

	a	Uniform points		Chebyshev points		Non-uniform points	
		Variable ε (min. ε, max. ε)	RMS error (Max.error)	Variable ε (min. ε , max. ε)	RMS error (Max.error)	Variable ε (min. ε , max. ε)	RMS error (Max.error)
Test problem 3	10^{-2}	(0.0831, 3.0182)	2.66(−3) (2.68(−2))	(0.0062, 3.1637)	1.87(−3) (1.15(−2))	(0.0843, 3.0140)	8.75(−4) (3.00(−3))
	10^{-3}	(0.5003, 1.1502)	8.25(−2) (7.29(−1))	(0.1054, 1.4600)	1.08(−2) (1.28(−1))	(0.1143, 2.4999)	2.49(−3) (1.62(−2))
	10^{-4}	(0.15003, 1.9953)	1.55(−1) (8.98(−1))	(0.5000, 4.3623)	7.66(−1) (1.67(+1))	(0.5000, 3.5630)	8.80(−3) (2.50(−1))
Test problem 4	10^{-2}	(0.1018, 3.0499)	3.08(−3) (2.26(−2))	(0.0077,3.0499)	2.09(−3) (8.25(−3))	(0.0805, 3.0499)	1.20(−3) 5.63(−3)
	10^{-3}	(0.1229, 2.4996)	1.18(−1) (7.29(−1))	(0.1294, 3.4999)	1.59(−2) (1.21(−1))	(0.1108, 2.4999)	1.36(−3) (1.20(−2))
	10^{-4}	(0.2099, 2.2499)	5.68(−1) (2.44)	(0.1257, 2.4996)	2.05(−1) (1.59)	(0.2578, 2.4999)	1.03(−2) (1.07(−1))

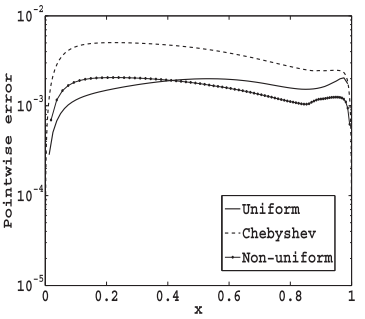

(a) Along $y = 0.95$, at $a = 10^{-2}$

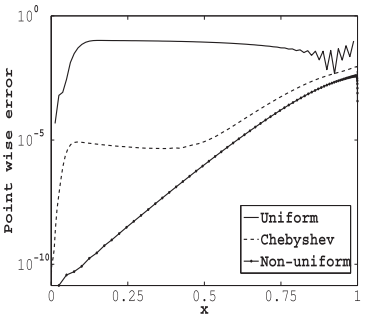

(b) Along $y = 0.95$, at $a = 10^{-3}$

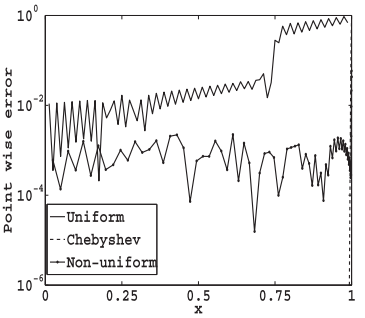

(a) Along $y = 0.25$, at $a = 10^{-4}$

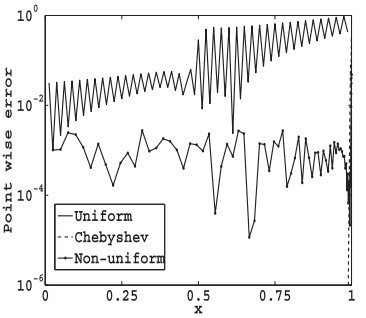

(b) Along $y = 0.50$, at $a = 10^{-4}$

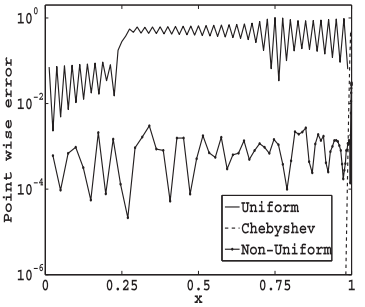

(a) Along $y = 0.75$, at $a = 10^{-4}$

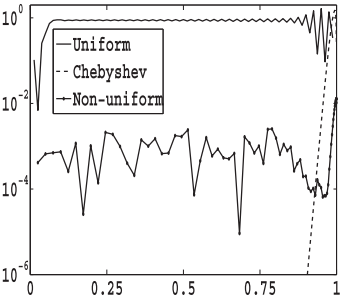

(b) Along $y = 0.95$, at $a = 10^{-4}$

Fig. 18. Comparison of pointwise errors, for the Test problem 4, $N = 81 \times 81$.

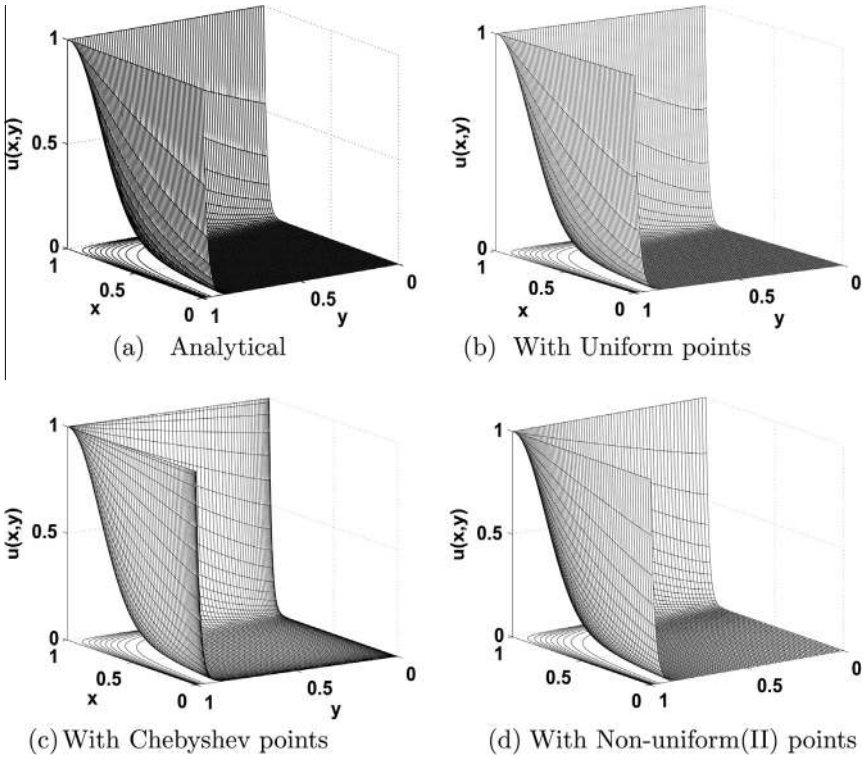

Fig. 19. Comparison of analytical and numerical solutions for the Test problem 4, at $a = 10^{-3}, N = 81 \times 81$.

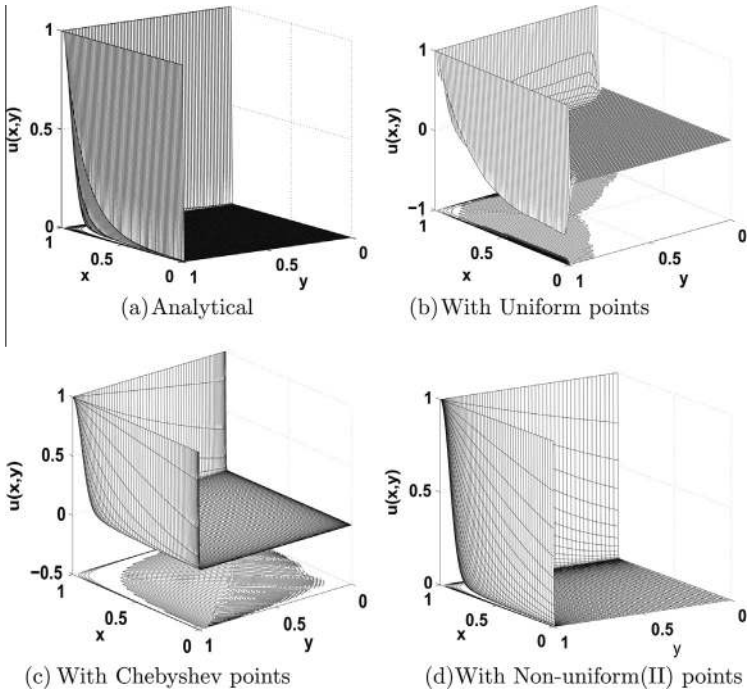

Fig. 20. Comparison of analytical and numerical solutions for the Test problem 4, at $a = 10^{-3}, N = 81 \times 81$.

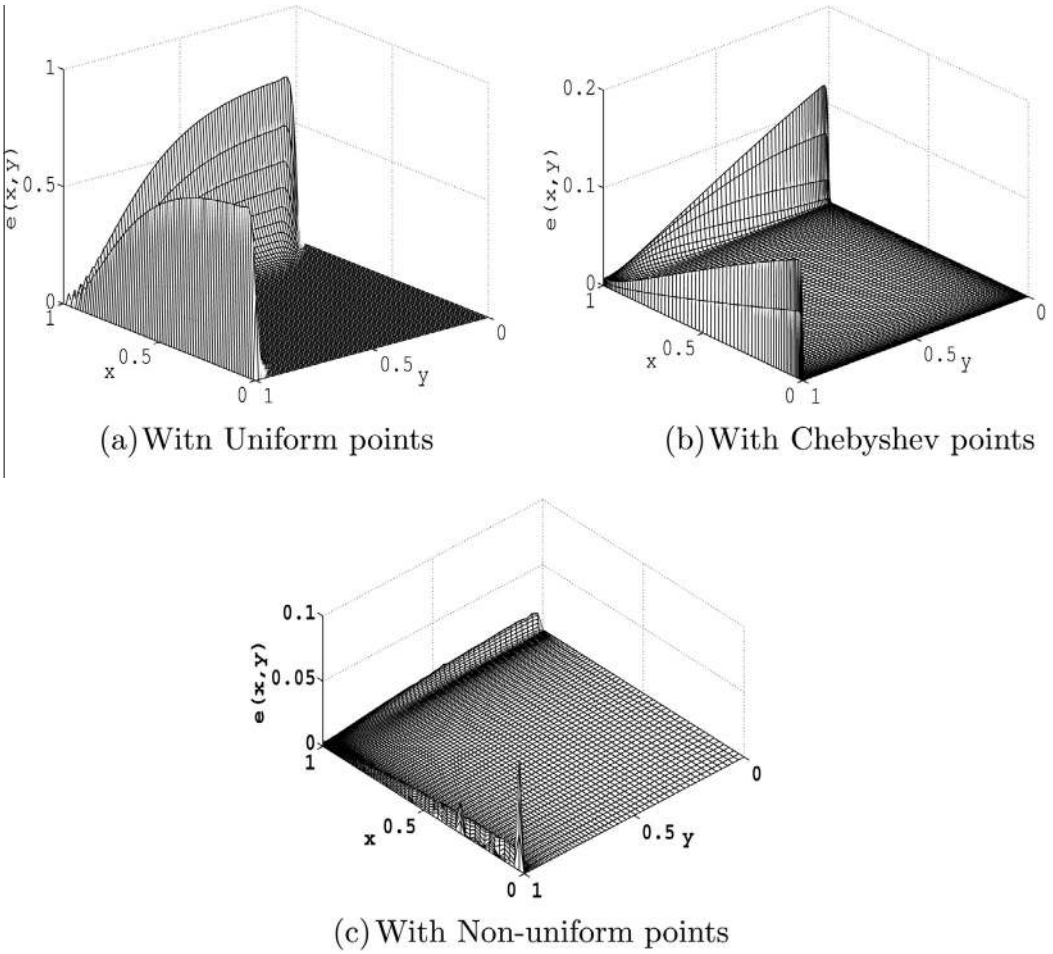

Fig. 21. Comparison of point wise errors for the Test problem 4, at $a = 10^{-3}, N = 81 \times 81$.

are presented in Fig. 21. It is clear from this figure that, in the boundary layer region, the errors in the solutions with uniform points is five times more with respect to the solution with the Chebyshev points and ten times more with the nonuniform points. Another important observation of this plot is the symmetric nature of the raise in the errors in the boundary layers of both x and y directions.

When the diffusion parameter is reduced to 10^{-4}, the point wise errors presented in Fig. 18 for various values of y show that the point wise errors with Chebyshev points are almost zero in most of the region except in the vicinity of $x = 1$. The nonuniform solution is marginally oscillatory and the uniform solution has the maximum errors particularly in the layer region. The inaccuracy of the solutions with uniform and Chebyshev points is also reflected in the comparison of numerical and analytical solutions presented in Fig. 22. When the nonuniform solution once again nicely mimicked the analytical solution, the other two have shown substantial deviation in the layer regions. To highlight the magnitude of the errors, the point wise errors in the whole domain for all the three cases are presented in Fig. 23. This figure shows that the errors with the nonuniform points are once again many times better than the other two. The quantitative comparison of the mean and maximum errors for all the three point distributions can be seen in the Table 6. The corresponding, minimum and maximum values of the variable optimal shape parameter are also reported in this table.

Once again, to highlight the performance of the scheme with variable shape parameter, a comparison of RMS and maximum error norms at different (fixed) shape parameters are compared with the errors obtained with variable shape parameter in Table 7 for both problems 3 and 4. The constant shape functions are chosen in the region wherein the scheme supposed to be more accurate. Its clear from these comparisons that, when nonuniform points are used, there is a two orders improvement for problem 3 and one order improvement for problem 4 while not much improvement is seen with uniform points. For Chebyshev points, in problem 3, there is an improvement of one order however, there not much change for problem 4. With in the variable shape parameter, the solutions with nonuniform points are two orders better than the other two for problem 3 and at least one order better for problem 4.

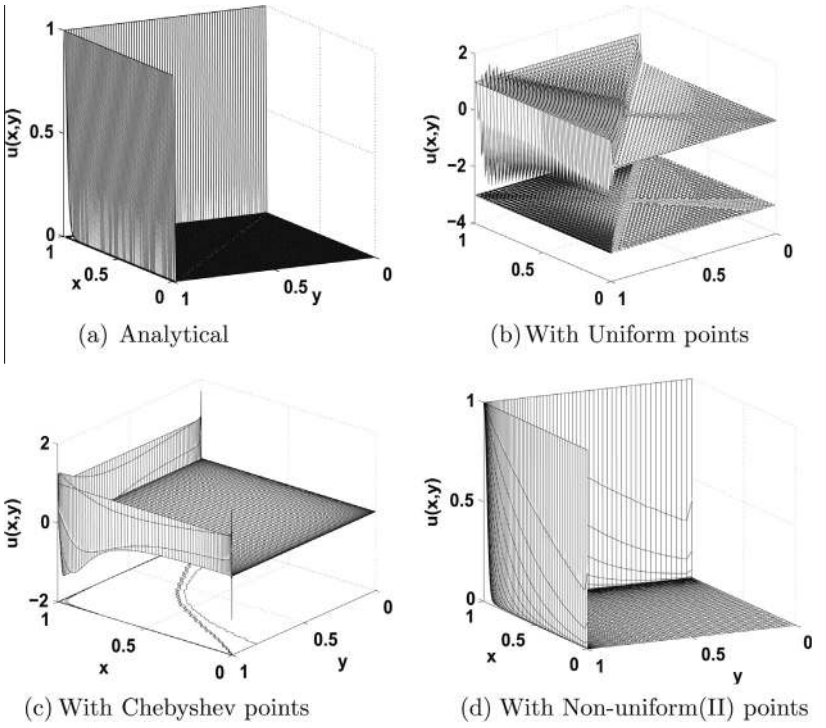

Fig. 22. Comparison of analytical and numerical solutions for the Test problem 4, at $a = 10^{-4}, N = 81 \times 81$.

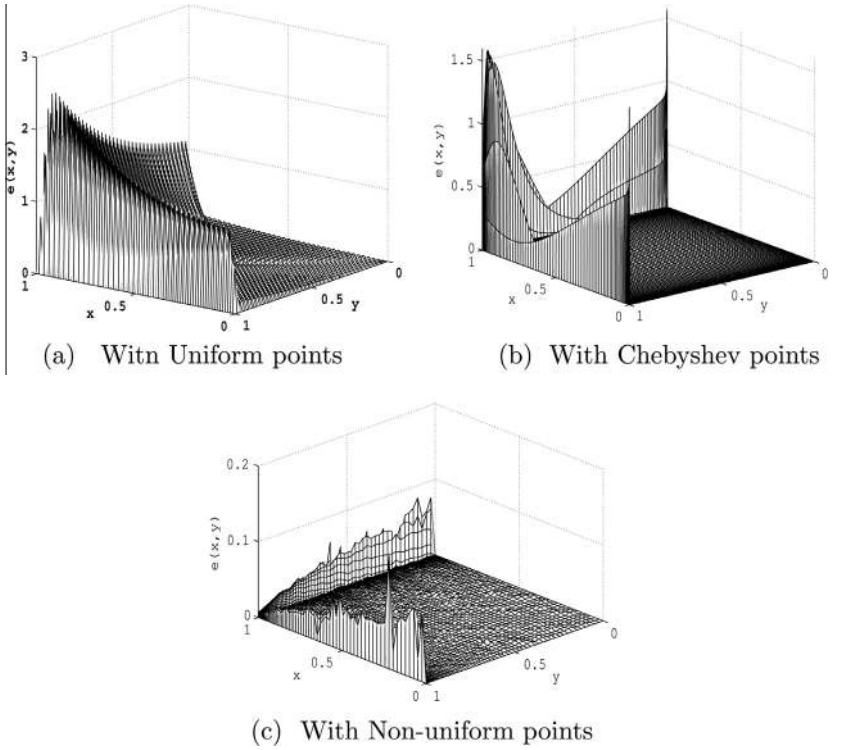

Fig. 23. Comparison of point wise errors for the Test problem 4, at $a = 10^{-4}, N = 81 \times 81$.

Table 7
Comparison of maximum and RMS errors computed with a fixed shape parameter at $a = 10^{-4}, N_x \times Ny = 81 \times 81$.

	ε	Uniform points		Chebyshev points		Non-uniform points	
		RMS error	Max. error	RMS error	Max. error	RMS error	Max. error
Test problem 3	0.1	3.35(−1)	1.14	1.66	4.68	1.02	2.53
	0.5	3.35(−1)	1.14	1.62(+2)	4.55(+2)	5.25(−1)	1.41
	1.0	3.35(−1)	1.14	1.40(+2)	3.94(+2)	5.14(−1)	1.38
	1.5	3.35(−1)	1.14	1.40(+2)	3.94(+2)	5.14(−1)	1.38
	ε_{var}	1.55(−1)	8.98(−1)	7.66(−1)	1.67(+1)	8.80(−3)	2.50(−1)
Test problem 4	0.1	5.68(−1)	2.44	2.04(−1)	1.57	3.20(−1)	1.40
	0.5	5.68(−1)	2.44	2.04(−1)	1.57	3.25(−1)	1.39
	1.0	5.68(−1)	2.44	2.04(−1)	1.57	2.58(−1)	1.36
	1.5	5.68(−1)	2.44	2.04(−1)	1.57	2.57(−1)	1.38
	ε_{var}	5.68(−1)	2.44	2.05(−1)	1.59	1.03(−2)	1.07(−1)

6. Conclusions

In this article, a local optimization algorithm to optimize the shape parameter of the infinitely smooth RBFs (multi-quadric in the present case) has been presented. The local optimization has been coupled with an RBF based local grid free (LRBF) scheme for solving highly convection dominated convection–diffusion equations. Uniform, Chebyshev and two sets of non-uniform point distributions have been considered, for solving some one and two dimensional test problems. Some of the important observations of the present work are:

- The optimization algorithm is based on the reconstruction of the forcing term of the CDE, therefore it depends on the problem under consideration and adjusts the shape parameter accordingly.
- It has been shown with verification that the (global) Cost function follows the (RMS) error function closely, therefore minimization of the cost function leads to the minimization of the error function. This has been observed for all the three types of the nodal distributions considered in the work.
- The comparison of the mean errors obtained using the LRBF scheme with the global, best and variable optimal shape parameters demonstrated that the LRBF scheme with the variable optimal shape parameter is most accurate among the all.
- For highly convection dominated problems, it is observed that the numerical solutions obtained over the uniform distribution of points are oscillatory than the other two nodal distributions.
- For smaller and smaller diffusion parameters, the accuracy with the nonuniform points, irrespective of constant or variable shape parameter, became better than the accuracy obtained with uniform and Chebyshev points.
- The error comparisons with fixed and variable shape parameters unveils that, the accuracy with Chebyshev and nonuniform points with variable shape parameter is many orders better, though the same is not reflected with the uniform points particularly at very low diffusion parameters.

Though the entire discussion in this work is centered around steady problems, the same can be extended to time dependent problems through method of lines.

Acknowledgement

The authors thank the reviewers for their valuable suggestions.

References

[1] M. Dehghan, M. Tatari, Determination of a control parameter in a one-dimensional parabolic equation using the method of radial basis functions, Math. Comput. Modell. 44 (2006) 1160–1168.
[2] M. Dehghan, A. Shokri, A numerical method for two-dimensional Schrodinger equation using collocation and radial basis functions, Comput. Math. Appl. 54 (2007) 136–146.
[3] M. Dehghan, A. Shokri, A numerical method for solution of the two-dimensional sine-Gordon equation using the radial basis functions, Math. Comput. Simul. 79 (2008) 700–715.
[4] M. Tatari, M. Dehghan, On the solution of the non-local parabolic partial differential equations via radial basis functions, Appl. Math. Model. 33 (2009) 1729–1738.
[5] M. Dehghan, A. Shokri, Numerical solution of the nonlinear Klein–Gordon equation using radial basis functions, J. Comput. Appl. Math. 230 (2009) 400–410.
[6] A. Shokri, M. Dehghan, A not-a-Knot meshless method using radial basis functions and predictor–corrector scheme to the numerical solution of improved Boussinesq equation, Comput. Phys. Commun. 181 (2010) 1990–2000.
[7] M. Tatari, M. Dehghan, A method for solving partial differential equations via radial basis functions: application to the heat equation, Eng. Anal. Boundary Elem. 34 (2010) 206–212.
[8] A. Shokri, M. Dehghan, A meshless method using radial basis functions for the numerical solution of two-dimensional complex Ginzburg–Landau equation, Comput. Modeling Eng. Sci. 84 (2012) 333–358.

[9] C. Shu, H. Ding, K.S. Yeo, Local radial basis function-based differential quadrature method and its application to solve two-dimensional incompressible Navier–Stokes equations, Comput. Methods Appl. Mech. Eng. 192 (3) (2003) 941–954.
[10] G.B. Wright, B. Fornberg, Scattered node compact finite difference-type formulas generated from radial basis functions, J. Comput. Phys. 212 (2006) 99–123.
[11] G. Chandini, Y.V.S.S. Sanyasiraju, Local RBF-FD solutions for steady convection–diffusion problems, Int. J. Numer. Methods Eng. 72 (2007) 352–378.
[12] Y.V.S.S. Sanyasiraju, G. Chandini, Local radial basis function based gridfree scheme for unsteady incompressible viscous flows, J. Comput. Phys. 227 (2008) 8922–8948.
[13] R. Franke, Scattered data Interpolation: test of some methods, Math. Comput. 38 (1982) 181–200.
[14] J.P. Boyd, The near equivalence of five species of spectrally accurate radial basis functions (RBFs): asymptotic approximations to the RBF cardinal functions on a uniform unbounded grid, J. Comput. Phys. 230 (2011) 1304–1318.
[15] R. Shaback, Error estimates and condition numbers for radial basis interpolation, Adv. Comput. Math. 3 (1995) 251–264.
[16] B. Fornberg, G.B. Wright, Stable computation of multiquadric interpolations for all values of the shape parameter, Comput. Math. Appl. 48 (2004) 853–867.
[17] B. Fornberg, C. Piret, A stable algorithm for flat radial functions over a sphere, SIAM J. Sci. Comput. 30 (2007) 60–80.
[18] B. Fornberg, E. Larsson, N. Flyer, Stable computations with Gaussian radial basis functions, SIAM J. Sci. Comput. 33 (2) (2011) 869–892.
[19] O. Davydov, D.T. Oanh, Adaptive meshless centers and RBF stencils for Poisson equation, J. Comput. Phys. 230 (2011) 287–304.
[20] E.J. Kansa, Multiquadrics – a scattered data approximation scheme with applications to computational fluid-dynamics – II: solutions to parabolic, hyperbolic and elliptic partial differential equations, Comput. Math. Appl. 19 (1990) 147–161.
[21] R.L. Hardy, Multiquadric equations of topography and another irregular surfaces, J. Geophys. Res. 76 (1971) 1905–1915.
[22] S. Rippa, An algorithm for selecting a good value for the parameter c in radial basis function interpolation, Adv. Comput. Math. 11 (1999) 193–210.
[23] E.J. Kansa, R.E. Carlson, Improved accuracy of multiquadric interpolation using variable shape parameters, Comput. Math. Appl. 24 (12) (1992) 99–120.
[24] B. Fornberg, Julia Zuev, The Runge phenomenon and spatially variable shape parameters in RBF interpolation, Comput. Math. Appl. 54 (2007) 379–398.
[25] G.E. Fasshauer, J.G. Zhang, On choosing optimal shape parameters for RBF approximation, Numer. Algor. 45 (2007) 345–368.
[26] R.M.C. Roque, A.J.M. Ferreira, Numerical experiments on optimal shape parameters for radial basis functions, Numer. Methods Partial Differ. Equ. 26 (3) (2010) 675–689.
[27] Y.V.S.S. Sanyasiraju, Chirala Satyanarayana, RBF based grid-free local scheme with spatially variable optimal parameter for steady convection – diffusion equations, CFD Letters 4 (4) (2012) 151–172.
[28] O. Davydov, D.T. Oanh, On the optimal shape parameter for Gaussian radial basis function finite difference approximation of the Poisson equation, Comput. Math. Appl. 62 (2011) 2143–2161.
[29] W.F. Spotz, G.F. Carey, Formulation and experiments with highorder compact schemes for nonuniform grids, Int. J. Heat Fluid Flow 8 (3) (1998) 288–303.
[30] E.C. Gartland, Discrete weighted mean approximation of a model convection–diffusion equation, SIAM J. Sci. Stat. Comp. 3 (1982) 460–472.